



# WPI

---

# HEAT TRANSFER DEMONSTRATION CART

---

## **A Major Qualifying Project**

Submitted to the Faculty  
of the  
**WORCESTER POLYTECHNIC INSTITUTE**  
in partial fulfillment of the requirements for the  
Degree of Bachelor of Science  
In Mechanical Engineering

### **Submitted By:**

---

Kyle LeBorgne

---

Foster Lee

---

João Maurício Vasconcelos

---

Robert Wood

**Date: April 21, 2016**

### Keywords

1. Heat Transfer
2. Flow Design
3. Instrumentation

### Approved:

---

Prof. Selçuk Güçeri, PhD, Project Advisor

## Abstract

Visual aids provide an opportunity for greater conceptual understanding in many engineering topics. In heat transfer education, such visualization tools are rare, if in practice at all. The objective of this project is to design and construct a portable device capable of both demonstrating heat transfer forced and natural convection in real-time, and measuring the convective heat transfer coefficient 'h'. Analysis of the design and functional requirements resulted in the development of a subsonic, insulated wind tunnel. The test chamber of the tunnel is outfitted with custom manufactured geometry and instruments including thermocouples and hot wire anemometry for data acquisition. Control of heat flux, air velocity, and test geometry enables the tunnel to simulate common sample problems found in introductory heat transfer textbooks. The successful operation of the experiment indicates the device is applicable to a broad range of configurations, including those that parallel introductory heat transfer problems.

## Executive Summary

The convective heat transfer coefficient ‘ $h$ ’, describes the rate at which heat moves between a solid geometry and the surrounding fluid. It is not a physical property of a material such as specific heat or thermal conductivity, nor is it a constant property of fluid dynamics. The coefficient is dependent on the type of media, gas or liquid, the flow properties such as velocity and viscosity, and other flow and temperature dependent properties. This concept, with its infinite variations, can be difficult to visualize and comprehend.

The objective of this project is to design and construct a portable device capable of both demonstrating heat transfer under forced and natural convection, and measuring the convective heat transfer coefficient ‘ $h$ ’. A visual aid of this nature provides an opportunity for greater conceptual understanding of Isaac Newton’s law of cooling. The control of heat flux, air velocity, and geometry will allow students to experiment with how changing these variables affect the transfer coefficient. This device will be applicable to a broad range of configurations, including those that parallel sample problems found in introductory heat transfer textbooks.



*Figure A 1: Completed Heat Transfer Demonstration Unit*

Analysis of the design and functional requirements resulted in the development of a subsonic, insulated wind tunnel. The test chamber of the tunnel is outfitted with a custom manufactured geometry and instruments including thermocouples and hot wire anemometry for data acquisition. The air velocity is controlled using a fan speed controller, and a hexagonal flow conditioner provides for flow uniformity and controls swirl. The test geometry is heated by a

3000 Watt variable autotransformer capable of warming the plate in excess of 400 degrees Celsius. The device is easily transportable, shown in Figure A1, functioning as a conceptual aid that can be brought to classrooms to enhance heat transfer education and also as a tool that will provide opportunities for future analysis.

From the experiments conducted during this project and the results our team collected, the relationship between the convective heat transfer coefficient and geometric orientation was interpreted, and conclusions were made about the behavior of 'h' as the controlled variables were manipulated. The team found that higher air velocities corresponded to higher rates of heat transfer between the two mediums, and subsequently, plate surface temperature decreased. The analysis of collected data determined that steeper slopes in the test geometry corresponded to higher rates of heat transfer and thusly higher values of 'h', as shown in Figure A2.

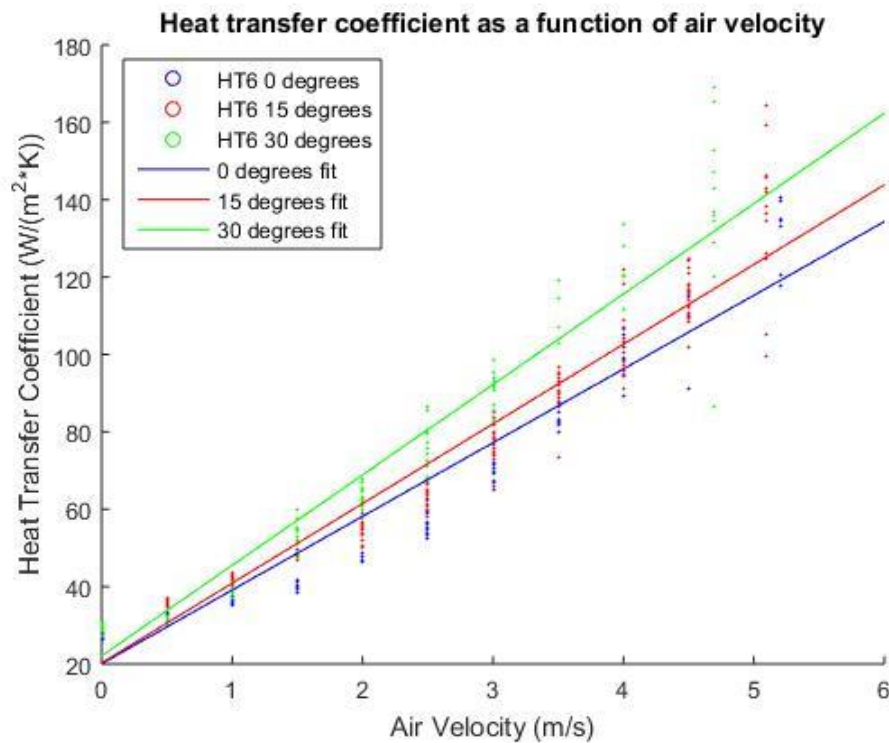


Figure A 2: Convective Heat Transfer Coefficient Results

We successfully completed the purpose of this project, demonstrating how to measure the convective heat transfer coefficient for given configurations within a university lecture hall.

## Acknowledgements

We would like to thank the following individuals and organizations for their support and contributions to the success of the project:

- Professor Selçuk Güçeri, PhD, for his continued guidance, enthusiasm, and support as our project advisor.
- Peter Hefti, Engineering Experimentation Lab Manager, for his support and supplying us with the necessary equipment to collect experimental data.
- Professor Jamal Yagoobi, PhD, and Mechanical Engineering Department Head, for providing the necessary equipment and financial support.
- Professor Alexander Emanuel, PhD, for his support with electrical component selection and instrumentation recommendations.
- Christopher Scarpino, Adjunct Instructor, for assisting with LabVIEW programming.
- Patricia Howe, Operations Manager, for providing our team with project working space.
- Barbara Furhman, Administrative Assistant VI, for purchasing all of our supplies and processing reimbursement payments.
- Aspen Aerogels for donating Pyrogel insulation for use on our project.
- Worcester Polytechnic Institute for making our experience on this project possible.

## Table of Contents

Abstract .....	i
Executive Summary .....	ii
Acknowledgements .....	iv
Table of Figures .....	3
Table of Tables .....	4
Chapter 1: Introduction .....	5
Chapter 2: Background .....	7
2.1 Methods of Heat Transfer .....	7
2.1.1 History of the Convective Heat Transfer Coefficient .....	7
2.1.2 The Convective Heat Transfer Coefficient .....	8
2.1.3 Flow, Boundary Layers, & Convective Heat Transfer .....	8
2.1.4 Textbook Approach to Experimentally Determine Heat Transfer Coefficients .....	10
2.2 Previous Heat Transfer Coefficient Experiments .....	12
2.2.1 Comparison of two methods for evaluation fluid to surface heat transfer coefficients	12
2.2.2 High Pressure Die Casting Experiment .....	12
2.3 Applications of the Convective Heat Transfer Coefficient.....	13
2.3.1 Aerospace Industry .....	13
2.3.2 High Pressure Die Casting .....	14
2.3.3 Heating, Ventilation, and Air Conditioning.....	15
2.3.4 Food Industry .....	15
2.4 Inspiration for this MQP .....	16
2.5 Active Learning in Engineering Education.....	16
2.5.1 History of Active Learning .....	17
2.5.2 Heat Transfer Courses.....	18
2.5.3 Heat Transfer Experiments .....	18
Chapter 3: Methodology .....	21
3.1 Subsonic Wind Tunnel Design .....	21
3.1.1 Design Process .....	21
3.1.2 Introduction to Subsonic Wind Tunnels .....	24
3.1.3 Research.....	25

3.1.4 Computational Testing.....	29
3.1.5 Design Limitations.....	33
3.2 Measurement and Instrumentation.....	34
3.2.1 Thermocouples.....	35
3.2.2 Hot-Wire Anemometer .....	37
3.2.3 LabVIEW and DAQ Box.....	37
3.3 Experimentation.....	40
3.3.1 Circuit Configuration.....	40
3.3.2 Experimental Procedures .....	40
Chapter 4: Results and Analysis .....	47
4.1 MATLAB Prediction and Experimental Result for $\Delta T$ vs. Power .....	47
4.2 MATLAB Prediction vs. Experimental Data.....	49
4.3 Plate Orientation Angle Experiment.....	50
4.4 Power vs. Heat Transfer Coefficient Experiment.....	51
4.5 General Heat Transfer Coefficient Experiment Data.....	52
4.6 Possible Sources of Experimental Error .....	53
Chapter 5: Conclusion and Recommendations .....	54
References.....	55
Appendix A: Construction .....	57
Appendix B: Instrumentation and Unit Setup.....	62
Appendix C: LabVIEW Program.....	68
Appendix D: Data Files .....	71
Appendix E: Additional MATLAB Generated Result's Graphs .....	73
Appendix F: ANSYS Generated Fluent Report.....	76
Appendix G: Textbook Sample Problem.....	87

## Table of Figures

Figure 1: Flat Plate in Parallel Flow (Bergman, Levine, Incropera, Dewitt, 2011).....	9
Figure 2: Example Honeycomb Laminar Flow Straightener Courtesy of Saxonpc.com .....	10
Figure 3: Boeing's Autoclave. Source: aviation-images.com .....	14
Figure 4: Example Applet Activity from Tan & Fok, 2009 .....	19
Figure 5: Example results from figure 4 above by Tan & Fok, 2009.....	19
Figure 6: Early Design Iteration .....	23
Figure 7: Nozzle CAD Image .....	27
Figure 8: Diffuser CAD Image .....	27
Figure 9: Final CAD Assembly .....	28
Figure 10: Three Dimensional Vorticity Simulation .....	29
Figure 11: Velocity vs Distance.....	30
Figure 12: Pressure vs Distance.....	31
Figure 13: Velocity Profile .....	31
Figure 14: Pressure Gradient .....	32
Figure 15: Turbulence Check.....	33
Figure 16: Thermocouples positioned according to letter type .....	36
Figure 17: Frame of one stacked sequence gathering data for one thermocouple.....	38
Figure 18: Calculation of the heat transfer coefficient in the LabVIEW program .....	39
Figure 19: Write-to-file and tab labels on block diagram.....	39
Figure 20: Variac Circuit Configuration.....	40
Figure 21: 15 Degree Orientation Angle .....	44
Figure 22: 30 Degree Orientation Angle .....	45
Figure 23: Predicted Q as a Function of $\Delta T$ and Air Velocity .....	48
Figure 24: Experiment Results: Q as a Function of $\Delta T$ and Air Velocity .....	48
Figure 25: At left, predicted $\Delta T$ vs. 'h'. At right, Experimental data $\Delta T$ vs. 'h'. .....	49
Figure 26: Experimental data $\Delta T$ vs. 'h' superimposed onto predicted $\Delta T$ vs. 'h' .....	49
Figure 27: 'h' as a Function of Air Velocity.....	50
Figure 28: 'h' as a Function of Air Velocity and Power.....	51

## Table of Tables

Table 1: Thermocouple Types .....	36
Table 2: General 'h' Coefficients for Air Velocity and Power .....	52

## Chapter 1: Introduction

As the demand for highly skilled workers and engineer's increases, so does the need to educate up and coming generations in the most effective way possible. In an age where there is so much to learn in only four years of high level schooling, finding the best ways to present information to students is key. Getting hands on experience and witnessing the magic of modern science not only reinforces understanding but excites and inspires students to discover.

The objective of this project is to design and construct a portable device capable of both demonstrating heat transfer under forced and natural convection, and measuring the convective heat transfer coefficient 'h'. A visual aid of this nature provides an opportunity for greater conceptual understanding of Isaac Newton's law of cooling. The control of heat flux, air velocity, and geometry will allow students to experiment with how changing these variables affect the transfer coefficient. This device will be applicable to a broad range of configurations, including those that parallel sample problems found in introductory heat transfer textbooks. The device is easily transportable, functioning as a conceptual aid that can be brought to classrooms to enhance heat transfer education and also as a tool that will provide opportunities for future analysis.

The heat transfer coefficient is an essential building block of thermodynamics. Without the study of its properties we could not have modern tools and technologies. Construction of air plane wings, easy access to food in the marketplace, and the ability to heat and cool our environment all require mathematical computation to estimate this 'h' value.

The convective heat transfer coefficient, 'h', changes drastically under different conditions. It is not a physical property of a material such as specific heat or thermal conductivity, nor is it a constant property of fluid dynamics. The coefficient is dependent on the type of media, gas or liquid, the flow properties such as velocity and viscosity, and other flow and temperature dependent properties. In simple terms, it describes the rate at which heat moves between a solid geometry and the surrounding fluid. This concept, with its infinite variations, can be difficult to visualize and comprehend. This is the primary motivation behind our project and why visual demonstration was taken into account in the design process. Our team will also include recommendations for future development and research opportunities.

This paper will introduce the fundamental elements of heat transfer and the equations that govern the convective heat transfer coefficient. It will discuss the experiments our team conducted and include an analysis of the relationship between the controlled variables and the convection coefficient. We will outline our procedure for designing our project, how we constructed it, and our approach to experimentally investigating the properties of 'h'. Data from the experiments our team conducted will be discussed and analyzed, and conclusions will be drawn from our results.

## Chapter 2: Background

To develop an enhanced understanding of heat transfer experiments, research of several experimental methods provided a foundation upon which an experimental design could be prepared. The following research and background information will provide insight into fundamental concepts, methods, and previous experiments. To begin, research on general heat transfer and the convective heat transfer coefficient including its history, proved meaningful when understanding design constraints. Additional detailed research into boundary conditions affects, previous experimental efforts, and convective applications provides validity to the research project. Lastly, investigation into active learning in engineering education pertaining to how this particular project will create opportunities in WPI's classrooms for generations.

### 2.1 Methods of Heat Transfer

Heat transfer is the process of thermal energy transfer due to a temperature difference in a medium or mediums. “Whenever a temperature difference exists in a medium or between media, heat transfer must occur” (Bergman, Lavine, Incropera, Dewitt, 2011). There are three conventional methods of heat transfer: conduction, convection, and thermal radiation. Conduction occurs where heat is transferred across a medium. Convection refers to heat transfer between a solid surface and a moving fluid. Heat transferred between mediums by way of electromagnetic waves is called thermal radiation. Any surface at a fixed temperature emits energy in the form of electromagnetic waves. (Bergman, Lavine, Incropera, Dewitt, 2011)

#### 2.1.1 History of the Convective Heat Transfer Coefficient

“Isaac Newton is widely credited with the following statement of the convective heat transfer coefficient:

$$q = hA(T_{sur} - T_{surr})$$

Where  $q$  is the rate of heat transfer,  $h$  the heat transfer coefficient,  $A$  the surface area,  $T_{sur}$  the surface temperature, and  $T_{surr}$  the temperature of the surroundings (Bergles 1988)”. Isaac Newton was a pioneer in the field of heat transfer, publishing papers in the early eighteenth century. Newton published a paper in 1701 that included the formula above. The historical accuracy of the statement above is under criticism from many scientists because Newton's paper does not specifically identify a proportional constant between heat flux and temperature

difference. The equation is often referenced as “Newton’s Law of Cooling”, leading to the conclusion Newton was instrumental in the development of convective heat transfer coefficient.<sup>1</sup>

### 2.1.2 The Convective Heat Transfer Coefficient

The heat transfer coefficient,  $h$ , is an essential quantity used in the calculation of heat transfer, generally used when there is a phase change between a fluid and a solid, or convection. The coefficient is not a physical property such as specific heat or thermal conductivity, but rather a descriptive quantity based on fluids interacting with geometries. As a fluid moves across a geometry, an extremely thin layer of the fluid “sticks” to the surface, resulting in heat transferring between the two mediums. “The convective heat transfer coefficient depends on conditions in the boundary layer, which are influenced by surface geometry, the nature of fluid motion, and an assortment of fluid thermodynamic and transport properties. Any study of convection ultimately reduces to a study of the means by which  $h$  may be determined” (Bergman, Lavine, Incropera, Dewitt, 2011). To determine  $h$  for critical components the calculation needs to be completed experimentally.

The convective heat transfer coefficient can be isolated, represented by the equation below.

$$\text{Convective Heat Transfer Coefficient} = h = \frac{q}{A(T_{sur} - T_{surr})}$$

The variable “ $q$ ” is the convective heat flux, representing the proportional difference between the temperatures of the surface,  $T_{sur}$ , and the surrounding area,  $T_{surr}$ . The SI standard units for  $h$ , is watts per square meter kelvin  $W/(m^2 \cdot K)$ .

### 2.1.3 Flow, Boundary Layers, & Convective Heat Transfer

The two methods of convective heat transfer include natural and forced convection. In natural convection the fluid surrounding the hot surface is not moving by an external force, rather the buoyancy force created by the temperature gradient causes the motion. In forced convection, the fluid is moving relative to the hot surface by an external force, for example a pump or fan. (Bergman, Lavine, Incropera, Dewitt, 2011) Flow refers to the motion of a fluid

---

<sup>1</sup> Enhancement of Convective Heat Transfer: Newton’s Legacy Pursued. Arthur E. Bergles.

over a surface with relatively velocity. Flow can be either laminar, layered flow without mixing between the layers, or turbulent, flow chaotic in nature with rapid property changes. The experiments conducted by our team will include flow across a heated flat plate, known as external flow. In external flow environments, there are no constraints imposed by adjacent surfaces, allowing boundary conditions to develop freely. (Bergman, Lavine, Incropera, Dewitt, 2011) “Despite its simplicity, parallel flow over a flat plate occurs in numerous engineering applications. Laminar boundary layer development begins at the leading edge and transition to turbulence may occur at a downstream location for which a critical Reynolds number is achieved” (Bergman, Lavine, Incropera, Dewitt, 2011). The figure below demonstrates how parallel flow moves across a flat plate.

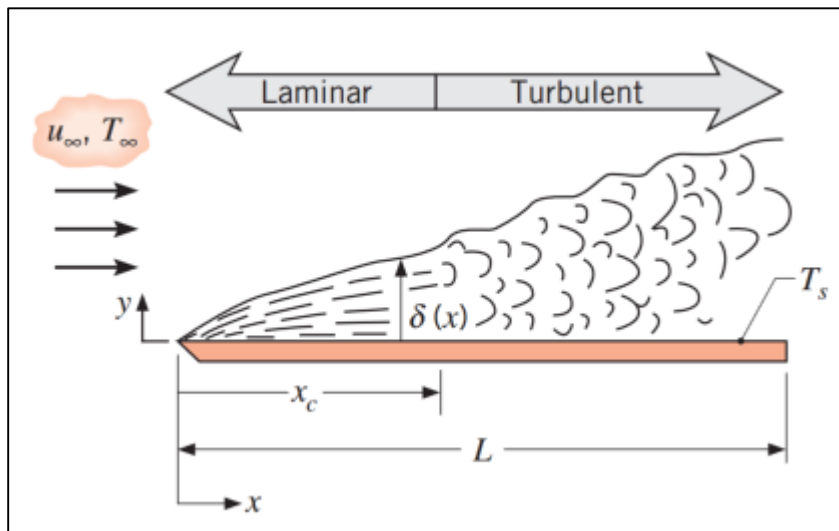


Figure 1: Flat Plate in Parallel Flow (Bergman, Levine, Incropera, Dewitt, 2011)

To achieve laminar flow at the entrance of the flat plate, a flow conditioner is placed upstream of the test section. The flow conditioner eliminates swirl and non-symmetry in the fluid by splitting the flow into numerous parallel conduits (Gallagher, 2005). The figure below displays a laminar flow straightener similar in structure to the honeycomb flow conditioner our team will be using.



Figure 2: Example Honeycomb Laminar Flow Straightener Courtesy of Saxonpc.com

Determining the convective heat transfer coefficient by varying the flow velocities, geometric angles, and temperatures will allow for numerous engineering application testing. Laminar flow is determined by the Reynolds number which will be explained in greater detail in the following section.

#### 2.1.4 Textbook Approach to Experimentally Determine Heat Transfer Coefficients

The following section is from the *Fundamentals of HEAT and MASS TRANSFER* Seventh Edition textbook commonly used in introductory heat transfer courses, including WPI. “The manner in which a convection heat transfer correlation may be obtained experimentally is illustrated in Figure 7.1. If a prescribed geometry, such as the flat plate in parallel flow, is heated electrically to maintain  $T_s > T_\infty$ , convection heat transfer occurs from the surface to the fluid. It would be a simple matter to measure  $T_s$  and  $T$ , as well as the electrical power,  $E * I$ , which is equal to the total heat transfer rate  $q$ . The convection coefficient  $\bar{h}_L$ , which is an average associated with the entire plate, could then be computed from Newton’s law of cooling, Equation 6.12. Moreover, from knowledge of the characteristic length  $L$  and the fluid properties, the Nusselt, Reynolds, and Prandtl numbers could be computed from their definitions, Equations 6.50, 6.41, and 6.42, respectively” (Bergman, Lavine, Incropera, Dewitt, 2011).

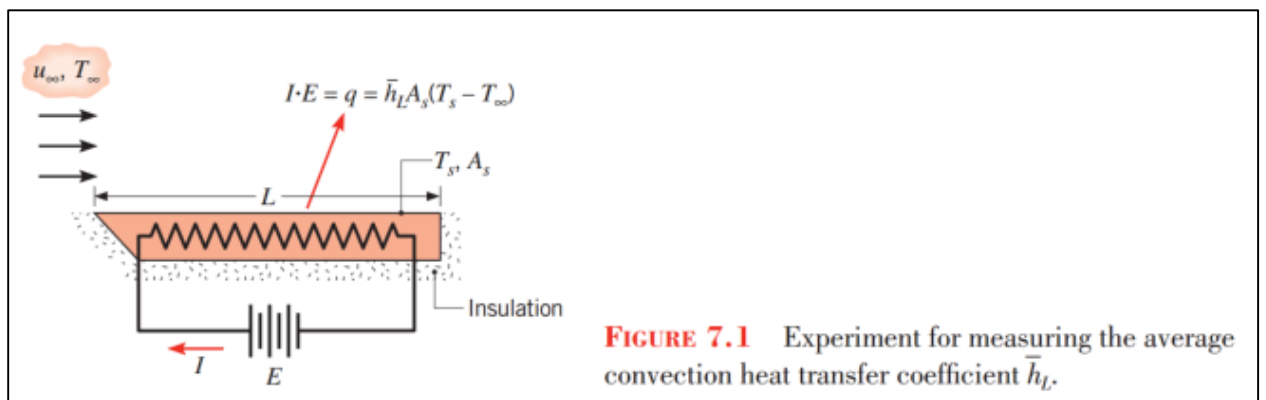
#### Required Procedure

1. Flat Plate Parallel Flow

2. Heated electrically to maintain  $T_s > T_\infty$
3. Then Convective Heat Transfer Occurs between the surface to the fluid
4. Measure
  - a.  $T_s = \text{Temperature on Surface of Flat Plate}$
  - b.  $T_\infty = \text{Temperature Before Flat Plate}$
  - c.  $E * I = \text{Power} = q$
  - d.  $A_s = \text{Area of surface}$
5.  $\bar{h}_L$  can then be computer by Newton's Law of Cooling

$$\bar{h}_L = \frac{q}{A_s(T_s - T_\infty)}$$

6. See Figure for visual representation



7. Nusselt, Reynolds, and Prandtl numbers can be then be computed

- a. Nusselt:  $N_u = \frac{\bar{h}_L * L}{K_f} = f(Re_L, Pr)$

“This parameter is equal to the dimensionless temperature gradient at the surface, and it provides a measure of the convective heat transfer occurring at the surface” (Bergman, Lavine, Incropera, Dewitt, 2011).

- b. Reynolds:  $Re_x = \frac{\rho u_\infty x}{\mu}$ ;  $x = \text{characteristic length for a flat plate}$

“The Reynolds number represents the ratio of the inertia to viscous forces” (Bergman, Lavine, Incropera, Dewitt, 2011).

- c. Prandtl:  $\frac{c_p \mu}{k} = \frac{\nu}{\alpha}$ ;  $\nu = \text{kinematic viscosity}, \alpha = \text{thermal diffusivity}$

“The Prandtl number is defined as the ratio of kinematic viscosity, also referred to as the momentum diffusivity,  $\nu$ , to the thermal diffusivity  $\alpha$ . It is therefore a

fluid property. The Prandtl number provides a measure of the relative effectiveness of momentum and energy transport by diffusion in the velocity and thermal boundary layers, respectively” (Bergman, Lavine, Incropera, Dewitt, 2011).

## 2.2 Previous Heat Transfer Coefficient Experiments

Discovered centuries ago, the heat transfer coefficient has been the focus of many previous research experiments conducted by large universities. Our team researched previous experimental methods; similar to the process we conducted, along with analytical methods to demonstrate alternative research techniques.

### 2.2.1 Comparison of two methods for evaluation fluid to surface heat transfer coefficients

An investigation conducted by the Department of Food Science and Agriculture at McGill University researched two analytical methods to accurately determine the convective heat transfer coefficients, while varying heating and cooling environments across three sample shapes (Awuah, Ramaswamy, Simpson, 1995). “Heat transfer coefficients are commonly evaluated from time-temperature data obtained from test objects of known shape, size and thermal properties. Of the two methods commonly used, both based on analytical solution to transient heat conduction equation, the first (rate method) is based on relating  $h_{fs}$  (Convective heat transfer coefficient ( $W/m^2\text{°C}$ )) to the rate of heating at a given location in the product. The second (ratio method) is based on relating  $h_{fs}$  to the temperature lag between two locations in the test object. Both methods require accurate thermophysical properties as input parameters” (Awuah, Ramaswamy, Simpson, 1995). The results illustrate similar  $h_{fs}$  values for experimentally identical conditions, particularly in situations where Biot numbers were low. The range of calculated values stretched between 15 and 420  $W/m^2\text{°C}$  depending on the test conditions (Awuah, Ramaswamy, Simpson, 1995). The report concluded, “Overall, the rate method gave more consistent and conservative  $h_{fs}$  values” (Awuah, Ramaswamy, Simpson, 1995).

### 2.2.2 High Pressure Die Casting Experiment

Our team’s goal to create an active learning approach to heat transfer courses, lead to design of a physical heat transfer experiment with a comparable method to the following study

funded by the National Science Foundation of China. “In this study, the IHTC (interfacial heat transfer coefficient) in the HPDC (high pressure die casting) process was determined based on the temperature measurements inside the die. The IHTC was then used as the boundary condition for the determination of the thermal field of the casting. Based on the simulated temperatures the pressure distribution inside the casting was determined. The metal/die interfacial heat transfer coefficient was successfully determined based on the measured temperature inside the die by solving the inverse heat transfer problem. The simulated results were found to be in reasonable agreement with the experimental data” (Guo, Xiong, Liu, Li, Allison, 2009).

## 2.3 Applications of the Convective Heat Transfer Coefficient

The coefficient is not a term only used by scientist in labs, or taught in engineering classes, it is relevant in numerous industries. The convective heat transfer coefficient has vital applications within the aerospace, food, HVAC, and metalworking industries. Any industry where media is heated or cooled will most likely estimate and use the convective heat transfer coefficient. The following are four examples of industries requiring frequent heat transfer.

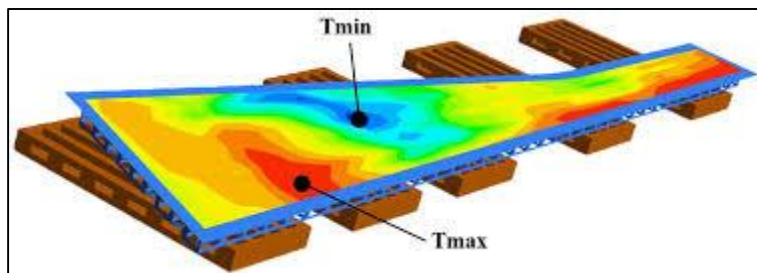
### 2.3.1 Aerospace Industry

Products of the aerospace industry have tremendous heat transfer requirements, and the calculations require accurate  $h$  values. Boeing, a leading passenger aircraft manufacturer, recently developed a predominantly carbon composite aircraft, the Boeing 787 Dreamliner. The carbon composite wings need to bake in an enormous autoclave to cure the epoxy resin and the carbon fibers. Aircraft manufacturers previously used machining to construct components, resulting in high waste costs. Current carbon fiber composite construction removes the machining process, allowing the manufacture to shape the material to exact component specifications, removing waste from the process. Each wing needs to bake as one unit, and contains millions of dollars' worth of carbon fiber composite. The convective heat transfer coefficient is a crucial value, which needs to be calculated experimentally to determine proper curing of the composite. The 787's wing demonstrates the sophisticated and financially significant implications in correctly determining the convective heat transfer coefficient between a fluid and surface. The image below demonstrates the enormity of Boeing's autoclave.



Figure 3: Boeing's Autoclave. Source: aviation-images.com

Temperatures can vary greatly between points on a surface undergoing thermal stresses. When Boeing uses heat to cure its aircraft wings, local minimum and maximum temperature values form on the surface of the wing. The graphic below demonstrates an example temperature distribution of a model aircraft wing, displaying the differences in maxima and minima in temperature.



### 2.3.2 High Pressure Die Casting

High Pressure Die Casting (HPDC) is rapidly becoming the leading method for producing aluminum and magnesium alloy components in industry. The HPDC method is extremely efficient and allows for alteration of the alloy's microstructure to improve component performance. "During the solidifications process, the microstructure of the casting is highly

dependent on the heat transfer process (which is characterized by the interfacial heat transfer coefficient (IHTC) at the metal/die interface” (Guo, Xiong, Liu, Li, Allison, 2009).

### 2.3.3 Heating, Ventilation, and Air Conditioning

The overall heat transfer coefficient (U-value) is crucial to determine how heat is transferred between a building envelope and the outside environment. The U-Value is comprised of the individual convective heat transfer coefficients of each fluid present in the system, examples include air inside the building, air outside the building, and air in-between window glass if more than one plane is present. Additional components include the thermal conductivity and thickness of the building envelope materials and the contact areas. “The knowledge of the U-Value is a precondition for the classification of the energy performance of existing buildings” (Fokaides, Kalogirou, 2011). While the convective heat transfer coefficient is only a portion of the overall coefficient, it does have significant implications in HVAC and building performance.

### 2.3.4 Food Industry

“The surface heat transfer coefficient  $h$  is a key parameter in the calculation of heating/chilling time, and hence in the design of facilities for thermal treatments of foods (hydro-cooling, air-cooling, cooking, etc.)” (Cuesta, Lamua, Alique, 2011). The food industry often uses large refrigeration and freezing units to chill foods to a lower temperature in preparation for storage or transportation. The refrigeration units, commonly referred to as chillers, use natural convection when fans do not assist circulation. Convection is significant when hot surfaces are exposed to cooler ambient air, commonly found in all facets of the food industry. When material is placed into the oven, and when material is removed from oven, convection significantly influences cooking and cooling of the material. “The increased consumer demand for high quality, nutritious and safe products at affordable prices has resulted in a need to minimize the severity of heat treatments without compromising safety” (Awuah, Ramaswamy, Simpson, 1995). Common kitchen techniques including baking, cooking, canning, steaming, and curing all require heat transfer leading to the development of new methods for determining thermal processes.

## 2.4 Inspiration for this MQP

The heat transfer course required for a Mechanical Engineering major at WPI is lecture based. The class does not include a lab section where hands-on heat transfer experiments can be conducted. Our team believes hands-on learning is essential for the modern student to entirely comprehend subject matter. WPI's motto is "Lehr und Kunst", German for theory and practice; however, a majority of the engineering science classes do not incorporate a practical element to the course. Upon further investigation and discussion with university officials, limited adequate lab space on campus is the primary reason for the deficiency in practical hands-on experiments. The principal motive for this MQP was to create an experimental unit that will allow students enrolled in WPI's heat transfer courses to perform experiments within the classroom. The idea of a demonstration unit was conceived during a discussion with Professor Guceri where he asked students for feedback on his heat transfer course. Professor Guceri was interested in student suggestions to improve the course in the future.

Our team is creating a device that will bring the laboratory to the classroom and expose students to theory and practice simultaneously, allowing for comprehensive active learning content and demonstrations to be incorporated in introductory heat transfer courses.

## 2.5 Active Learning in Engineering Education

Active learning is a relatively new approach to teaching at the higher educational institutions. Active learning involves students participating in course by doing more than just listening; therefore, "They must read, write, discuss, or be engaged in solving problems. Most important, to be actively involved, student must engage in such higher-order thinking tasks as analysis, synthesis, and evaluation" (Bonwell, Eison, 1991). Traditional learning environments involve a formal lecture from a professor; students are engaged in the lecture by listening and recording notes. "Research has demonstrated, for example, that if a faculty member allows students to consolidate their notes by pausing three times for two minutes each during a lecture, students will learn significantly more information (Ruhl, Hughes, and Schloss 1987). Two other simple yet effective ways to involve students during a lecture are to insert brief demonstrations or short, ungraded writing exercises followed by class discussion" (Bonwell, Eison, 1991).

### 2.5.1 History of Active Learning

Active learning became a widely used and accepted approach to education in 1991 when Charles C. Bonwell and James A. Eison published *Active Learning: Creating Excitement in the Classroom*. The United States Department of Education Office of Educational Research and Improvement sponsored the research and was featured in the Association for the study of Higher Education and published by The George Washington University School of Education and Human Development. Active learning faced many barriers at first, most notably from faculty members and institutions who had perceptions on what higher education means and the traditions associated with it. Instructors and professors did not have incentives to change curriculum, as well as the anxiety and discomfort created by change itself (Bonwell, Eison, 1991). “The reform of instructional practice in higher education must begin with faculty members’ efforts...Faculty can successfully over-come each of the major obstacles or barriers to the use of active learning by gradually incorporating teaching strategies requiring more activity from students and/or greater risk into their regular style of instruction” (Bonwell, Eison, 1991). Throughout the following decades after the publication of Bonwell and Eison’s report, active learning slowly began to enter higher education courses. The advance of technology in classrooms increased the availability of active learning methods to faculty; therefore, leading to adoption of active learning at many major institutions including Worcester Polytechnic Institute.

Research studies conducted on active learning show promising evidence to the merit behind the theory of active learning. University physics courses were among the early adopters of the active learning approach, with numerous major studies displaying supporting statistical evidence. A survey of 6,542 students in 62 introductory physics courses, showed the 48 courses using active learning, or interactive engagement techniques, improved student scores by 25 percent to reach an average gain of 48 percent with a standard deviation of 14 on the Force Concept Inventory, the standard test of physics conceptual knowledge (Hake, 1998). The 14 courses, which did not participate in active learning techniques, achieved an average gain of 23 percent with a standard deviation of four (Hake, 1998). Additionally, a report published by the American Association of Physics Teachers explains, “When instructors switched their physics classes from traditional instruction to active learning, student learning improved 28 percent points, from around 12% to over 50%, as measured by the Force Concept Inventory, which has

become the standard measure of student learning in physics courses” (Hoellwarth, Moelter, 2011).

### 2.5.2 Heat Transfer Courses

Active learning in undergraduate heat transfer courses has been a topic of discussion for The American Society of Mechanical Engineers (ASME). At the 2008 ASME Summer Heat Transfer Conference, there were several presentations on new and innovative approaches to introductory heat transfer courses. Michael Pate presented one technique, often practiced in courses at WPI, “The method focuses on minimizing lecture time and maximizing student engagement. Learning is achieved by forming small groups of two to three students who then work on in-class graded assignments” (ASME, Pate, 2008). Heat transfer courses at WPI use group projects and in-class assignments to stimulate learning and generate greater outcomes. Our project aims to advance active learning objectives with real-time experiments and physically illustrate the concepts explained in the textbook.

### 2.5.3 Heat Transfer Experiments

One approach to developing interactive projects for heat transfer and thermal courses is through computer-based applets. The Nanyang Technological University (NTU) has been conducting research into active learning methods, with a focus on applets. “...Development of electronic resources for thermal-fluid courses, with a focus on the development of interactive learning activities for students to explore and discover heat transfer concepts and mechanisms. Three basic types of Java applets based on the three main types of interactive knowledge discovery activities” (Tan, Fok, 2009). The team at NTU created more than 30 different interactive simulations designed specifically to aid students understanding of the core principles of heat transfer. The figure below demonstrates an example applet that closely relates to our demonstration cart.

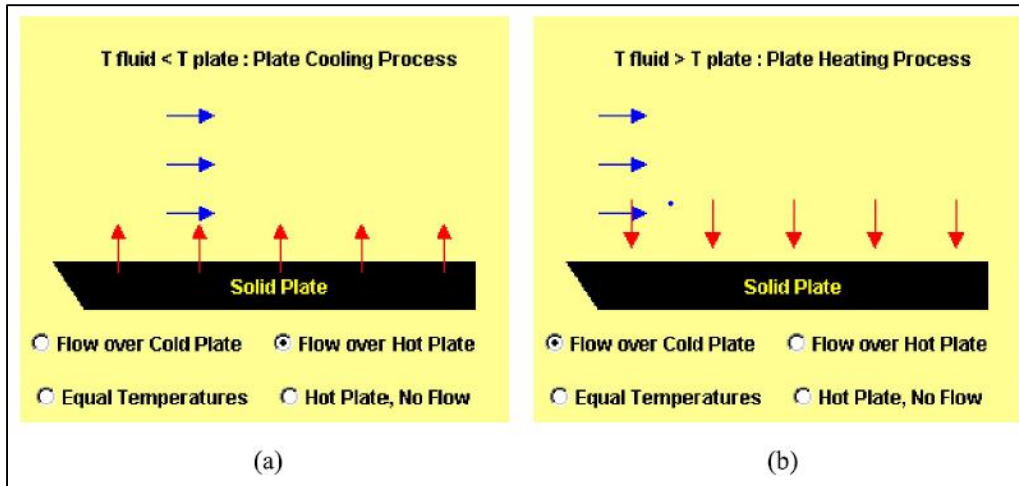


Figure 4: Example Applet Activity from Tan & Fok, 2009

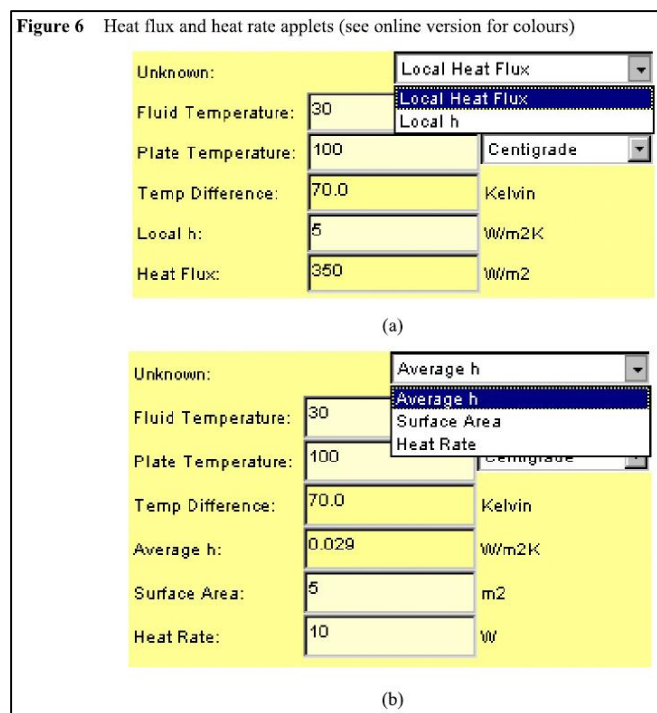


Figure 5: Example results from figure 4 above by Tan & Fok, 2009

“The evaluation from a small sample of students and staff on the developed interactive learning activities indicated that the activities can aid the students in the visualization of certain heat transfer concepts and can assist the student to acquire thermal knowledge through exploration” (Tan, Fok, 2009).

Using physical elements and real-time data collection will allow students to visualize crucial concepts in heat transfer and draw conclusions in new ways. Experiments created and

conducted using textbook examples will add a new level of validity to the hypothetical problems students are asked to solve. Students will gain valuable experimental skills using advanced instrumentation including thermocouples, hot wire anemometers, inferred thermometers, and variac transformers. We firmly believe the addition of a heat transfer demonstration cart will change introductory heat transfer courses at WPI and contribute to the advancement of active learning methods.

## Chapter 3: Methodology

### 3.1 Subsonic Wind Tunnel Design

#### 3.1.1 Design Process

The heat flux caused by forced convection is given by the following equation:

$$Q_{conv} = hA(T_s - T_{inf})$$

Where  $Q_{conv}$  is heat flux,  $h$  is the convective heat transfer coefficient,  $A$  is surface area,  $T_s$  is surface temperature, and  $T_{inf}$  is ambient temperature. With knowledge of this equation, it can be easily understood that by controlling heat flux via controlling input power to a system, recording surface area of a test configuration, and measuring both configuration surface temperature and ambient temperature, an experiment can be carried out for the purpose of finding the heat transfer coefficient 'h' for that specific configuration.

Axiomatic design was utilized for the purpose of defining project requirements. Axiomatic design is a design methodology requiring matrices to lay out independent functional requirements of a design, and link them to design parameters and process variables (Suh, 1990). The link between functional requirements and design parameters is visualized in the equation below.

$$\begin{bmatrix} FR1 \\ FR2 \end{bmatrix} = [A] \begin{bmatrix} DP1 \\ DP2 \end{bmatrix}$$

Where the A matrix is known as the design matrix.

In designing this project, functional requirements, or FRs, and design parameters, or DPs, were used to eliminate poor designs early in the design process.

The functional requirements for the system are as follows:

FR1: The system must be capable of experimentally measuring the heat transfer coefficient 'h' for configurations that parallel sample heat transfer textbook problems.

FR2: The system must not noticeably affect the ambient conditions of the room in which it is operated.

Where the rooms ambient conditions are comprised of temperature, noise to a reasonable degree, and air velocity to a reasonable area of influence should air be used as the systems convective medium. The design parameters were then selected to be the following:

DP1: The system will regulate input power, make use of configuration surface area, and measure surface and ambient temperatures.

DP2: The system shall be insulated and closed in sections that are likely to affect ambient conditions.

The first functional requirement, FR1, is broken down to the following elements:

FR11: The system must provide for laminar flow at the leading edge of the test geometry.

FR12: The system must allow for multiple configuration surface temperatures.

FR13: The system must allow for multiple convective medium velocities.

Likewise, the second functional requirement is then broken down.

FR21: The system must not noticeably affect the temperature of the environment in which it operates.

FR22: The system must not produce an uncomfortable amount of audible noise

Given these expanded functional requirements, design parameters are defined. The first design parameter, DP1, expands to the following:

DP11: Presence of a flow conditioning system that ensures laminar flow for the full range of convective medium velocities.

DP12: Installation of a user-controlled heating element tied to the test geometry capable of generating temperatures from at least room temperature to 200°C.

DP13: Installation of a user-controlled pump or fan for convective medium velocity control for a velocity range of at least .5 m/s to 5 m/s.

Similarly, the second design parameter expands to the following:

DP21: The system shall be insulated and closed in select areas such that the temperature immediately surrounding the system does not change by more than 3°C.

DP22: The system must not produce more than 85dBA of noise, which is the level at which hearing loss can potentially occur if exposure is prolonged (CDC/NIOSH, 1998).

After establishing expanded functional requirements and design parameters, several design iterations were drafted and measured based on their compliance with the established axioms.

The first design believed to fulfil each requirement and parameter can be seen in figure 10.

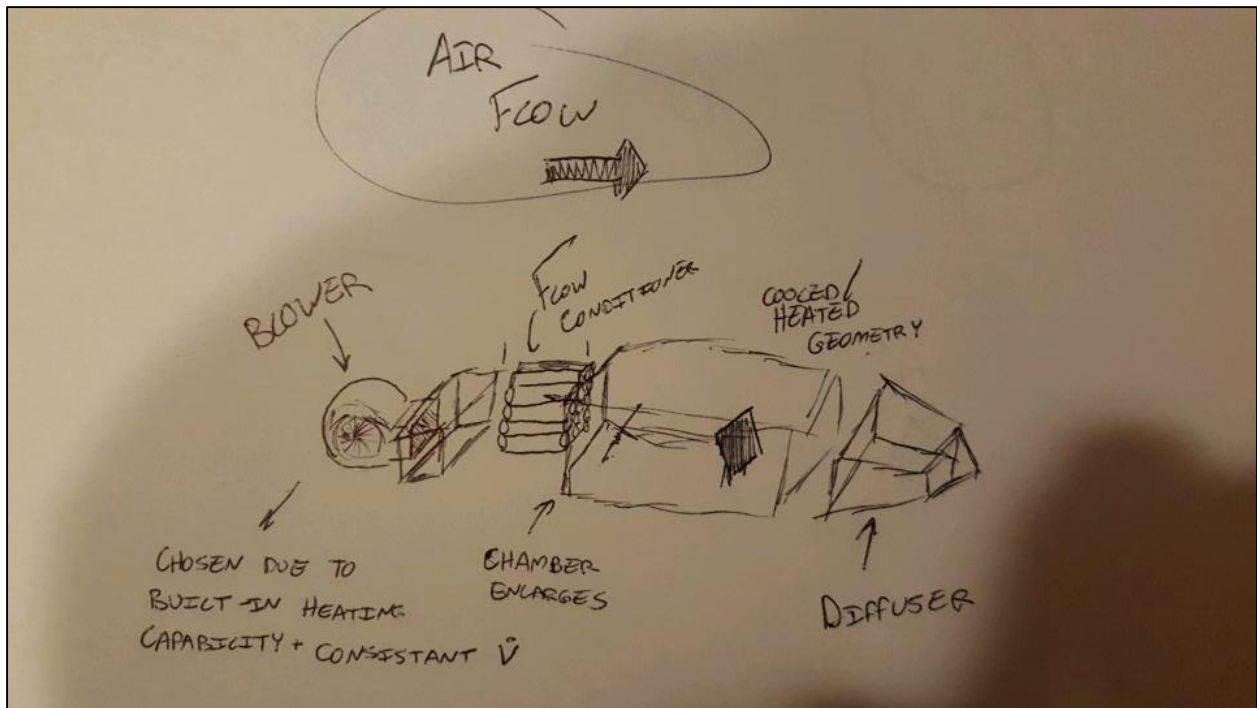


Figure 6: Early Design Iteration

The design shown in figure 6 very closely resembles a wind tunnel. It can be seen that this design forces air over a test geometry in a central test chamber via a centrifugal blower at the nozzle end of the tunnel, after this air is conditioned through a series of tubes. After the test geometry has been affected by the airflow, air exits the tunnel through a diffuser. Dimensioning this design lead to a roughly 5.5 foot long system, with three feet of that system being dedicated to the test chamber. The flow conditioner was chosen to be constructed from a series of thin walled metal tubes, where the metal would be chosen based on material cost. Finally, the nozzle

and diffuser were selected to be made from glass due to high temperature capabilities and relatively low material cost.

Dimensioning and computationally testing this design iteration resulted in an unfavorable conclusion. The material requirements for the test chamber, diffuser, and nozzle were found to be unrealistic due to the size and complex shape of each component, and for the instrumentation requirement that would require the glass to be drilled into. Computational testing found that the proposed flow conditioner was not capable of reducing swirl in airflow to acceptable levels.

Due to these shortcomings, the design was modified to accommodate the full range of requirements, while enabling ease of instrumentation implementation and controlling cost. The length of the design was extended to eight and a half feet to enable a larger nozzle and longer diffuser. The test chamber was altered from solid glass to an insulated wooden base with glass walls and a glass lid to more easily enable instrumentation to be installed. Likewise, the nozzle and diffuser were modified to be constructed from wood to control cost. Finally, to control swirl, the flow conditioner was chosen to be a honeycomb shape and the fan was changed to a suction fan located at the end of the diffuser. The design process behind each of these modifications is explained in section 3.1.3.

### 3.1.2 Introduction to Subsonic Wind Tunnels

Wind tunnels are devices used primarily to test the aerodynamics of a vehicle or vehicle component (Dunbar, 2014). By using wind tunnels, it is possible to assess how a gaseous substance behaves around a geometry. Air is the most common medium to be used in a wind tunnel.

Frank Wenham is widely considered to be the wind tunnel's inventor, with his twelve foot long tunnel constructed in 1871. Previously, methods for testing the aerodynamics capabilities of an object were either natural sources, such as the mouth of a windy canyon, or a device known as the Whirling Arm invented by the mathematician Benjamin Robins (Baals, 1981). The Whirling Arm was a mass-pulley system, which spun an arm as weight fell, with obvious limitations in the inaccuracy of data collection and the fact that the tested object was being propelled into its own stream.

Current applications of wind tunnels include aircraft testing with scale aircrafts, spacecraft testing, and automobile aerodynamics testing. Additionally, individual components of a system can be tested and analyzed using wind tunnels. Of course, some tunnels are large enough to accommodate and test full sized systems (Dunbar, 2014).

Wind tunnel applications concerning convective heat transfer are not a new idea – many studies have been conducted utilizing subsonic wind tunnels to test the heat transfer coefficients of both organic and manmade systems, such as plant leaves (Kumar, 1971) and airfoils for icing investigation (Kirby). Outside of research, thermal tunnels are employed in many industrial applications, such as engine cooling system examination in the automotive industry (“Thermal Wind Tunnel”). However, devices intended for educational aid are uncommon and difficult to find. The wind tunnel for this project was design using the design rules and practices from existing research based thermal wind tunnels, as well as design rules for general subsonic wind tunnels, as described in section 3.1.3.

### 3.1.3 Research

Due to the temperature requirement of the convective heat transfer experiment, a few requirements for the wind tunnel are readily obvious. The first being that the tunnel must be capable of withstanding the temperatures that will be generated within the test section, and thus the test section must be made from a material with an ability to withstand high temperatures, or must be insulated. The second is that data acquisition tools that normally would not be required in a wind tunnel must be used to collect data on how temperature is changing over time at various points of interest on the geometry. Due to budget constraints, these devices most likely would be thermocouples, and thus must be held in place in such a way that they consistently measure the same point regardless of convective medium speeds in the test section. These requirements predominantly affect the test section layout and material requirement, whereas the requirements for the nozzle, diffuser, flow conditioner, and fan follow those rules that apply to any subsonic wind tunnel.

The blower or fan requirement was driven predominantly by budget. Release of compressed air, which can be seen in some tunnels for short tests, could be eliminated due to both inconvenience of operation and limited test duration. Centrifugal blowers and axial fans were investigated, as they are common open loop wind tunnel components and can be acquired

for relatively low prices. Centrifugal blowers, present in the initial design iteration explained in section 3.1.1, are potential options for tunnels due to their consistent operation under a wide range of flow conditions, including varying power factor (Metha, 1979), which is of great interest to this experiment. Additionally, centrifugal blowers generally operate relatively quietly, which fulfils a design parameter defined in section 3.1.1. Axial fans are commonplace as well, and an axial fan was selected due to ease of installation and cost. This axial fan was selected and acquired based on cost, ease of installation, noise generation, and appropriate CFM rating.

Regardless of fan choice, the final design iteration was known to be a suction tunnel due to the potential that air coming from a room containing an open loop wind tunnel may be less prone to swirl or turbulence than air being forced via an inlet blower system (Metha, 1979).

The nozzle, located at the front of the tunnel before the test section and containing the flow conditioner, was designed first by selecting area ratio and then by selecting length, where area ratio is the ratio between the nozzle inlet area and the nozzle exit area. Metha (1979) states that an area ratio of six to ten should be chosen. This is done in order to minimize pressure losses. Because the system test chamber size had already been set to a minimum size of 1ft x 1ft x 3ft, the nozzle was constructed with a known outlet area of 1 square foot.

Length of the nozzle is chosen by the following equation:

$$1 \cong \frac{L}{2y_0}$$

Where L is length and  $y_0$  is half of the height of the nozzle inlet. The completed nozzle CAD file can be seen below in figure 7.

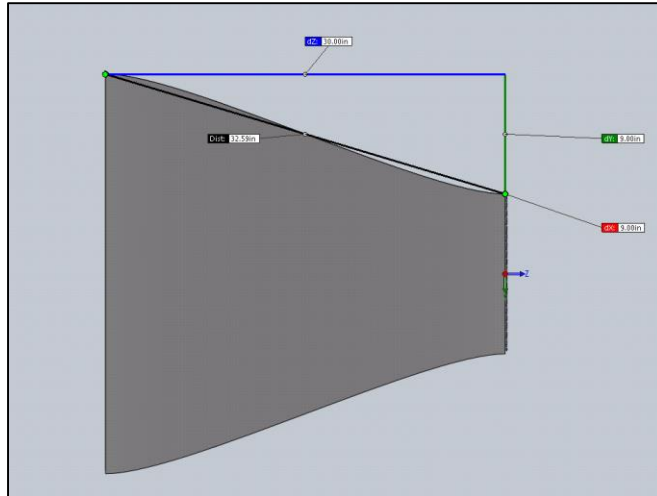


Figure 7: Nozzle CAD Image

The diffuser had a known inlet area of 1 square foot due to the test chamber specifications. According to Metha (1979), the expansion angle of the diffuser, mathematically represented as  $2*\theta$ , usually should not exceed five degrees and an area ratio of roughly 2.5. However, flow steadiness can be maximized at roughly a 10 degree expansion angle (Metha, 1979). The area ratio rule was applied, and the expansion angle was selected predominately to reduce length. The diffuser was tested computationally to ensure function due to the decision to reduce diffuser length via a higher expansion angle. The completed diffuser CAD file can be seen below in figure 8, where the diffuser inlet is to the right and has a cross sectional area equivalent to that of the test section.

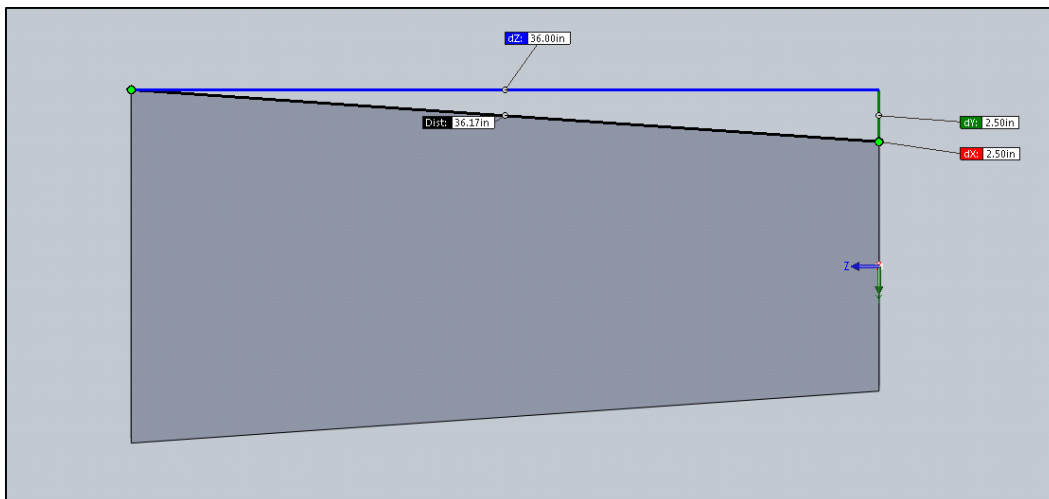


Figure 8: Diffuser CAD Image

An important metric in confirming the test chamber length of 1ft x 1ft x 3ft was the hydraulic diameter of the test chamber, which is defined as:

$$D_h = 2 * \sqrt{\frac{A}{\pi}}$$

Where  $D_h$  is hydraulic diameter and A is cross sectional area. According to Metha (1979), the length of the test chamber should be .5 to 3 times the hydraulic diameter, which is the case with the 1ft x 1ft x 3ft test chamber size.

The flow conditioner was chosen based on previously discovered problems with swirl in the initial design, as well as with budget constraints. In an effort to reduce swirl, a honeycomb flow conditioner was selected, as honeycomb conditioners are effective at reducing swirl (Metha, 1979).

Once each tunnel subsystem was dimensioned, Solidworks® was utilized for the production of the CAD files, which would be used to visually display what the system will look like once constructed, to serve as a production aid during system construction, and for later use within computational fluid dynamics software to confirm system conformity to flow requirements. The completed tunnel CAD image can be seen below in figure 9.

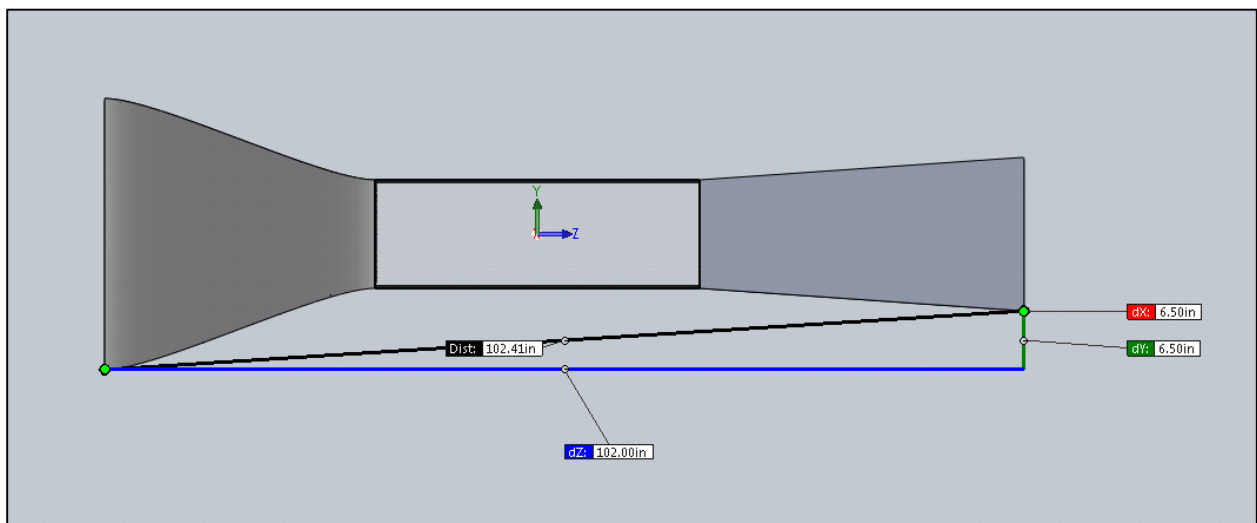
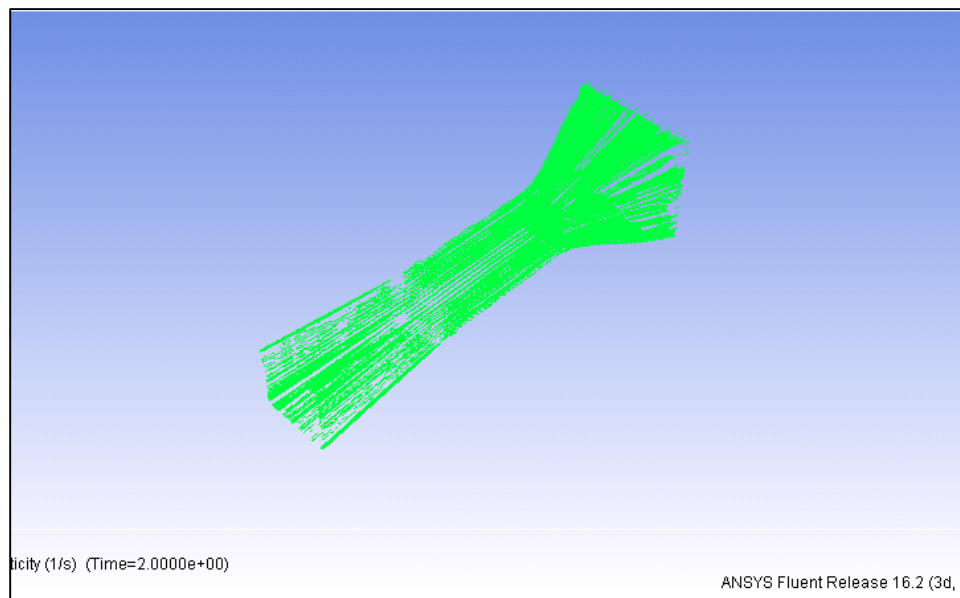


Figure 9: Final CAD Assembly

### 3.1.4 Computational Testing

In order to confirm that the system design behaved appropriately concerning airflow, particularly regarding air velocity and turbulence within the test chamber, ANSYS® Fluent® was utilized. The Solidworks® CAD file was exported as an .IGS file and imported into Fluent®. The full Fluent® report, which includes data on boundary conditions, mesh, and setup inputs for the final CFD iteration, can be found in appendix F. Figure 10, shown below, depicts vorticity results through the three dimensional tunnel.



*Figure 10: Three Dimensional Vorticity Simulation*

In order to lower simulation time, and to minimize human error in ANSYS® setup, a two-dimensional approximation was made regarding flow through the tunnel using ANSYS® Design Modeler®. It is important to note, however, that the 2D approximation does not include a honeycomb flow conditioner, and so results have potential to display a less uniform flow profile than the physical system produces.

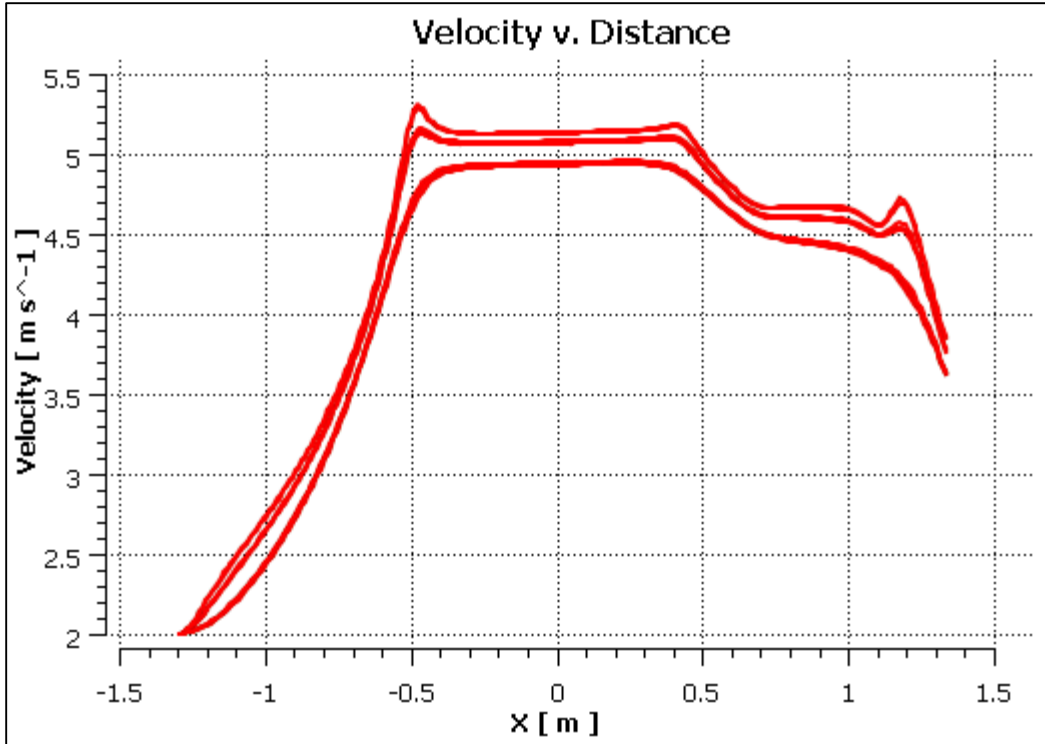


*Figure 11: Velocity vs Distance*

After the simulation had been set up with the known boundary conditions and fan speed at the end of the diffuser, the simulation ran for 1500 iterations, which was comfortably past the threshold of solution convergence. Figure 11 and figure 12 show the velocity profile and pressure profile of the tunnel over distance from the nozzle respectively. It is evident that the highest velocities occur in the test chamber, and succeed in meeting the minimum velocity set forth in the functional requirements and design parameters.

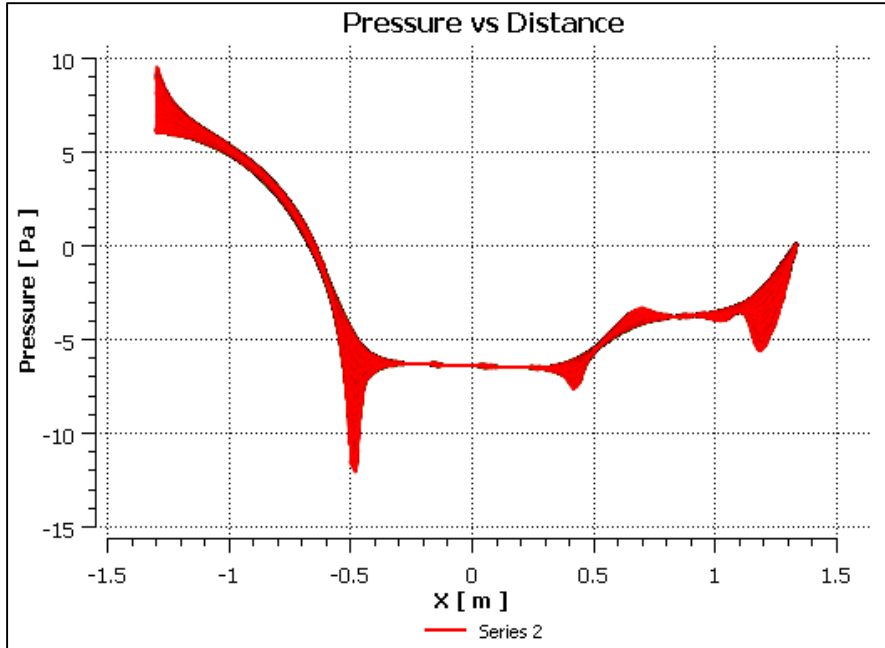


Figure 12: Pressure vs Distance

Velocity profile is also shown through the 2D Design Modeler® file below in figure 13. Again, it is evident that the appropriate air velocities are being met in each respective section of the tunnel, and even though the flow conditioner is not present in the 2D approximation, flow is still relatively uniform through the test section.

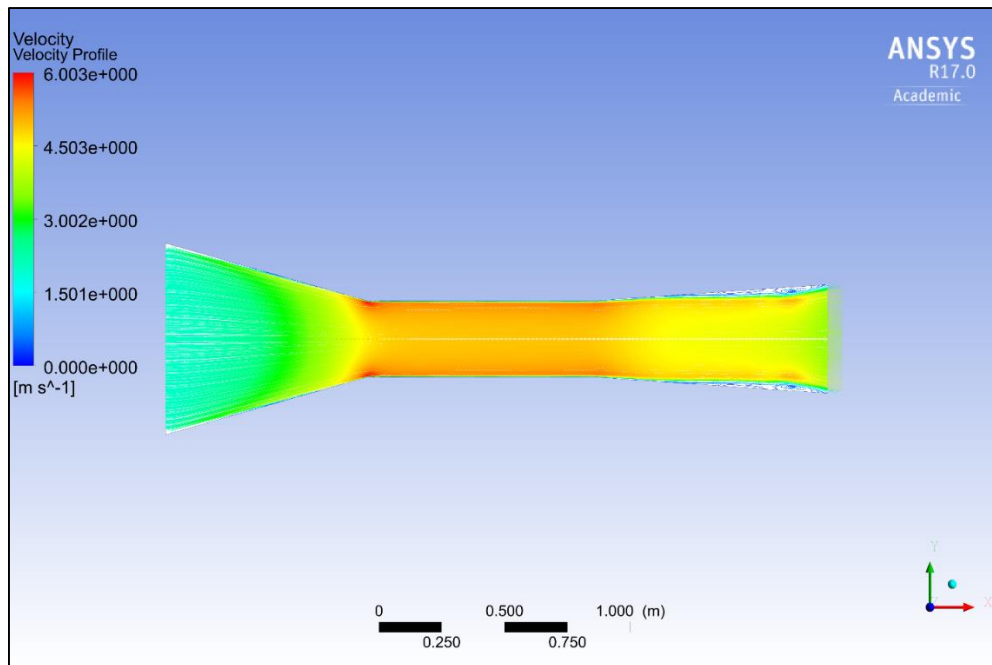


Figure 13: Velocity Profile

The tunnel pressure gradient, also an area of interest, is seen in figure 14 below. Observation shows that pressure is relatively low and constant through the test chamber, and peaks at the outlet of the nozzle.

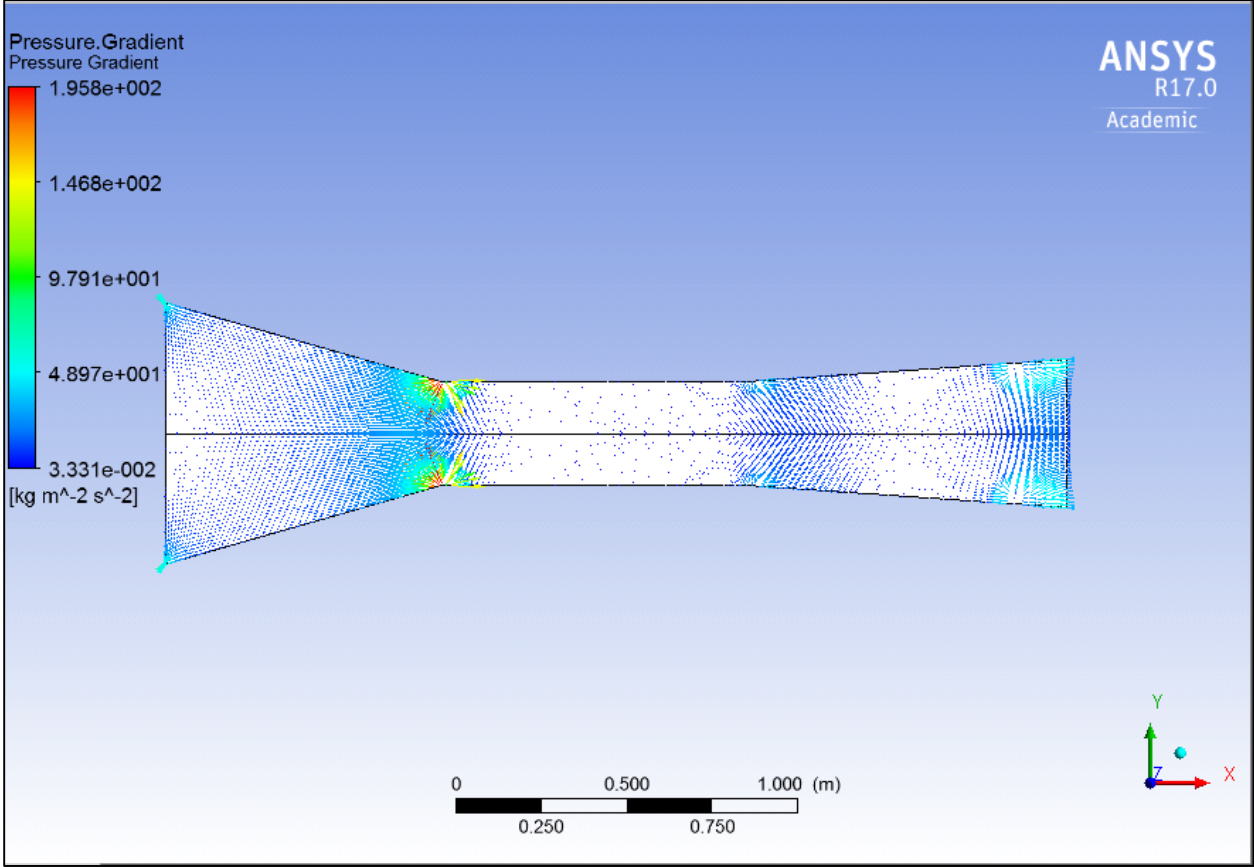


Figure 14: Pressure Gradient

Finally, streamlines were analyzed to ensure that swirl and turbulence were not issues with the tunnel design. The diffuser was an area of interest due to the shortened diffuser length, and the velocity profile and pressure gradient indicate that there is potential for swirl near the end of the diffuser.

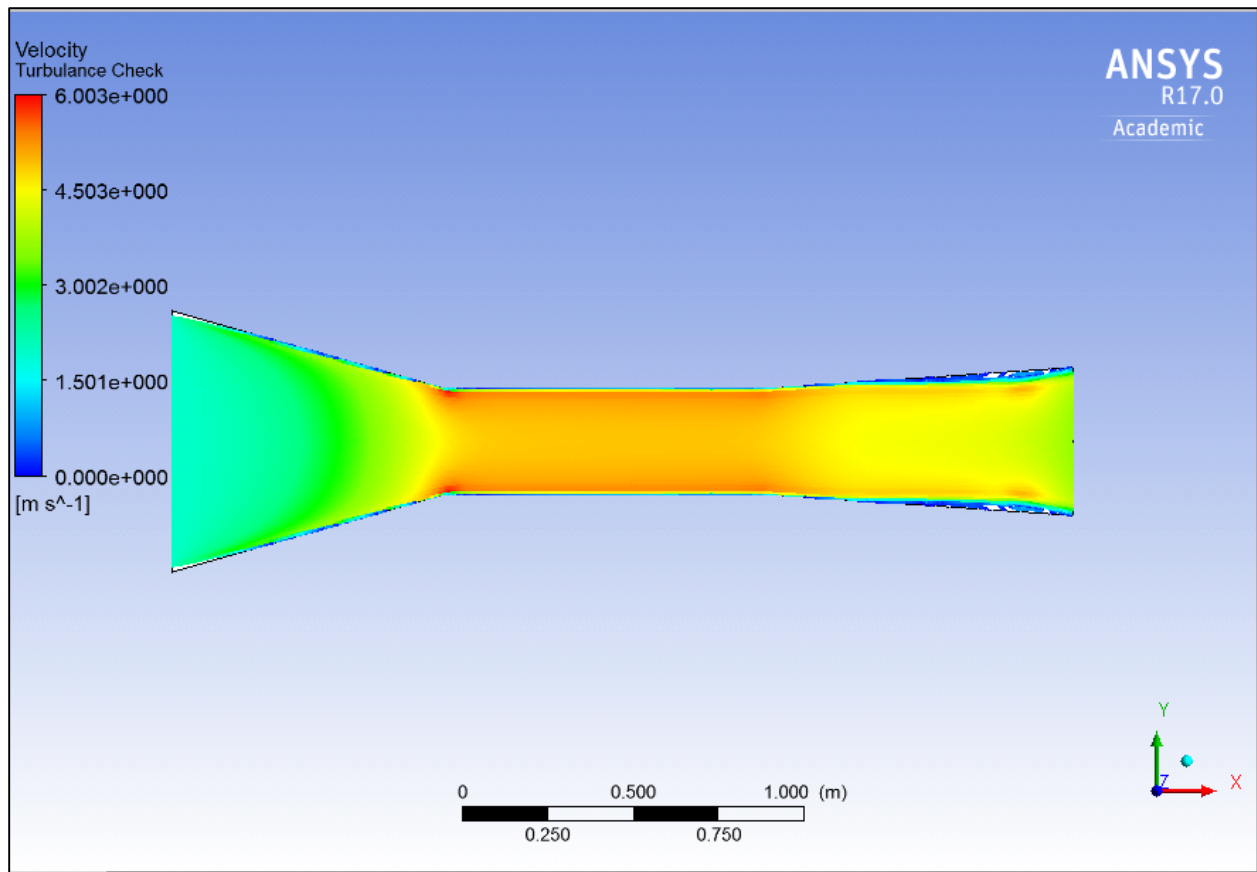


Figure 15: Turbulence Check

Figure 15 confirms that there is potential swirl near the end of the diffuser. However, as it is minimal, and thus likely does not have a significant detriment on the quality of flow within the test section, the shortened diffuser length in the interest of saving space could be deemed safe for this tunnels purpose.

### 3.1.5 Design Limitations

Given the functional requirements and design parameters that limit system size, noise generation, and ambient condition alteration, this tunnel has predictable limitations in the types of configurations that can be tested, as well as the velocity range a given configuration can be tested over. It is also the case that, based on the heating element used to heat geometry, as well as the presence and accuracy of selected instrumentation, that additional design limitations will be generated.

Computational test results indicate a maximum velocity between 5 and 5.5 meters per second, which is the first and most clear limitation of the tunnel. This makes any tests involving components exposed to higher speeds, such as automotive or aerospace components, or even components exposed to higher speed winds during storms or other natural sources, impossible to test. However, experimental data collected with this tunnel system can be trended to gain a sense of how the heat transfer coefficient will behave at air velocities close to the maximum tunnel speed.

Additionally, in respect to airflow, only laminar flow environments can be tested. Of course, realistically, not all flow that could be experienced by a geometry in practice is laminar. However, by testing laminar flow, it is possible to experimentally obtain a potential lower bound on the convective heat transfer of the test configuration for that flow environment, as laminar flow is less effective at forced convective heat transfer than turbulent flow (Patil, 2015).

In respect to instrumentation, the most readily apparent limitation is the accuracy and precision of the instruments themselves. Factors such as signal noise and general lack of accuracy to a high degree contribute to data acquisition limitation. It is also worth mentioning that, if uninsulated, the thermocouples themselves can potentially act as a heat sink, and thus can detract from the accuracy of the configuration surface temperature measurements.

Finally, the system heating element surface area is roughly  $0.04129 \text{ m}^2$ . Due to the inherent requirement for heat to be transferred to the geometry via conduction, tested configurations must be sized around to the size of the heating element. Insulation may also need to be adjusted depending upon the given test configuration.

### 3.2 Measurement and Instrumentation

This heat transfer demonstration device consists of various sub-systems that put together are capable of making room temperature airflow through the device and quickly heating it up through the test chamber. Most sub-systems are responsible for providing the conditions at which the convective heat transfer coefficient is found. For instance, the fan, diffuser and nozzle are responsible for the laminar air that goes into the test chamber, whereas the power generation sub-system and the heated plate are responsible for the heating of air. Yet, none of these portions of the project are really responsible for the measurement of 'h', the convective heat transfer

coefficient. A separate sub-system is required to measure the temperature of air and its velocity through the test chamber. These measurements are done by the instrumentation sub-system.

The instrumentation sub-system consists of the measurement tools and the LabVIEW program. The measurement tools consist of thermocouples and anemometers. These are simple and cheap devices that can be easily connected to the LabVIEW program. The computer software, LabVIEW, plays a major role in this project. In order for the experiments to have results in real-time, LabVIEW is required to continuously calibrate measurements and run calculations to find the value of 'h'. This section of the report deals with the instruments used to measure physical quantities in the test chamber and the software logic used to calculate the convective heat transfer coefficient.

### 3.2.1 Thermocouples

Thermocouples are temperature sensing devices that consist of two different types of metal wires welded together to produce small voltage differentials. These differentials occur due to the Seebeck Effect, which describes the continuous current flow in two connected wires of distinct metals. They can be measured and calibrated in order to electronically determine the temperature of surfaces and fluids.

There are different types of thermocouples. Each of the thermocouple types are distinguished by their temperature range and their sensitivity. Table 1 details thermocouples' temperature range and sensitivity. It is clear from the table that some thermocouples have better sensitivity and better temperature ranges. According to OMEGA, a global leader in the production of thermal sensors and other components, type K thermocouples are considered a multipurpose thermocouple due its large temperature range and low cost. Since this project deals with a fairly high temperature scale, it has been decided that type K thermocouples are the most applicable for large variations in temperature, such as the hot plate. Type T thermocouples are more accurate are more adequate for the measurement of the temperature of air or temperatures surrounding the plate. The protection cover of type T thermocouples is also different from that of K parts. T-type cover cannot withstand the temperature range of the experiments and therefore it must be safely positioned within the test chamber such that the heat of the plate does not overheat the device.

Table 1: Thermocouple Types

Thermocouple Type	Temperature Range (°C)	Standard Limits of Error (°C)
J	0 to 750	2.2
K	-200 to 1250	2.2
E	-200 to 900	1.7
T	-250 to 350	1.0

In total, this device uses seven thermocouples. Three of which are T-type and the other four, K-type. The schematic for this setup is depicted in Figure 16, where the green box is the test chamber and the gray box is the hot plate. Here, the letters T and K represent the type of the thermocouple used and its position on the plate or test chamber. Also, notice that every single thermocouple is labeled from T0 to T6. This setup was chosen in order to compare measured temperatures at the center of plate as well as the edges of the plate. The T thermocouples were lined up with the K thermocouples to ensure the temperature differential is calculated in the direction of airflow. Thus, there are four  $\Delta T$ 's:  $\Delta T_3 = T_3 - T_0$ ;  $\Delta T_4 = T_4 - T_1$ ;  $\Delta T_5 = T_5 - T_1$ ;  $\Delta T_6 = T_6 - T_2$ . These temperature differentials are used to calculate the convective heat transfer coefficient.

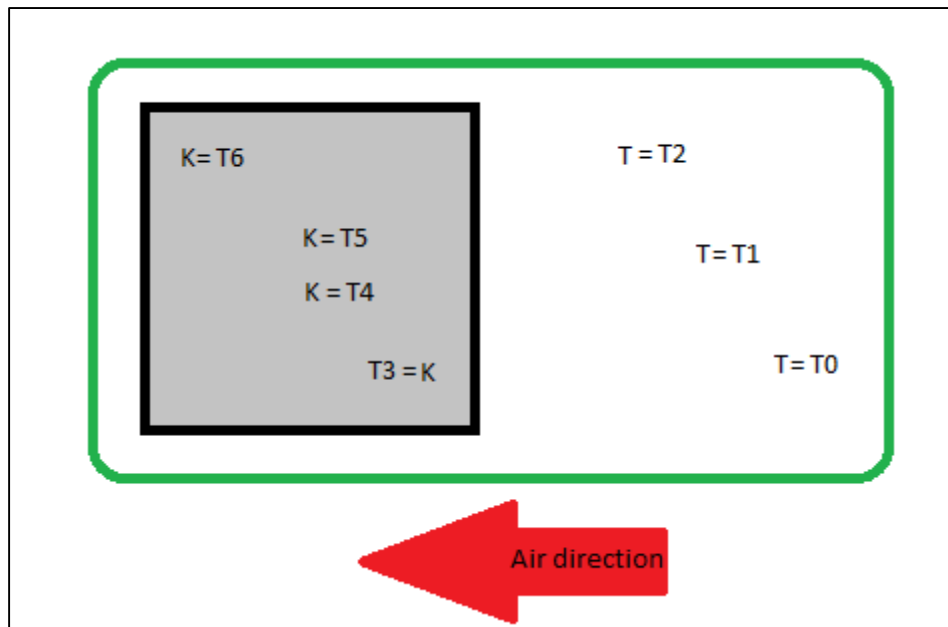


Figure 16: Thermocouples positioned according to letter type

### 3.2.2 Hot-Wire Anemometer

Anemometers are devices used to measure wind speed. Anemometers were primarily used for meteorological purposes and were gradually refined in both technology and application. The mechanical design of anemometers includes simple cup anemometers and windmill anemometers. Both of these anemometers use the wind speed to rotate a fan. Yet, cup anemometers rotate in the direction tangent to the wind vector, whereas windmill anemometers rotate orthogonally to the wind. Both of these can be connected to analog gauges to measure the speed of wind.

Hot-wire anemometers use a finer technology to accurately measure the velocity of air. They are part of a segment of anemometers commonly known as thermal anemometers and are mostly used in laminar to transition flow types. Hot-wire anemometers use a filament of wire that is kept at constant temperature due to a self-regulatory current through the wire filament. Once wind blows over the hot wire, it changes the temperature of the wire, which, through several internal flow calculations, determines the speed of air. Due to their high accuracy even in large air velocity ranges and their rather quick response, these devices are found in industrial applications.

The hot-wire anemometer, Testo 405i, was selected for this project (see Appendix B). Among other hot-wire anemometers, this was the most cost-effective solution for it uses a smartphone application to display its measurements. Even though this device is also used in industrial applications, it is significantly cheaper than other devices that have similar operations. It measures temperature and air velocity simultaneously and is capable of exporting all data in multiple formats!

### 3.2.3 LabVIEW and DAQ Box

While the thermocouples and the hot-wire anemometer deal with measurement of specific physical variables, the LabVIEW program and the Data Acquisition (DAQ) Box are responsible for converting the electric pulses from the physical channels into digital data. The DAQ Box (model NI-USB-6363) receives analog voltage variations from the thermocouples and uses its internal analog-to-digital converter to transform the analog voltage impulses into bits. It

is a 16-bit device with a maximum dynamic range of +/- 10V. Thus, the resolution is approximately 305.2 $\mu$ V/bit.

The LabVIEW program runs the data collection in this project. It is responsible for collecting the signal from the DAQ Box as well as running the program that calculates the heat transfer coefficient and outputting all of the data into excel files. The LabVIEW runs an endless while loop, which can only be stopped manually. This loop will continuously gather data from each thermocouple individually through a stacked sequence structure shown in Figure 17. Next, it will run data gathered from the thermocouples back into the loop in order to perform the calculation of four separate heat transfer coefficients. This feedback system and the calculation of the coefficient is depicted in Figure 18. Notice that, for the equation, two indicators are used for 'Power' and 'Area' and that the temperature for other thermocouples is fed back into the system after being delayed in time. This means that the orange symbol with an arrow represents a Z-transform, which means that the output is fed back into the system, but delayed one unit in time. This was used to internally calculate the heat transfer coefficient. Finally, Figure 19 details the portion of the block diagram in which the output is written to an excel file. Data is written to the excel file according to a delay time variable that is determined by the user.

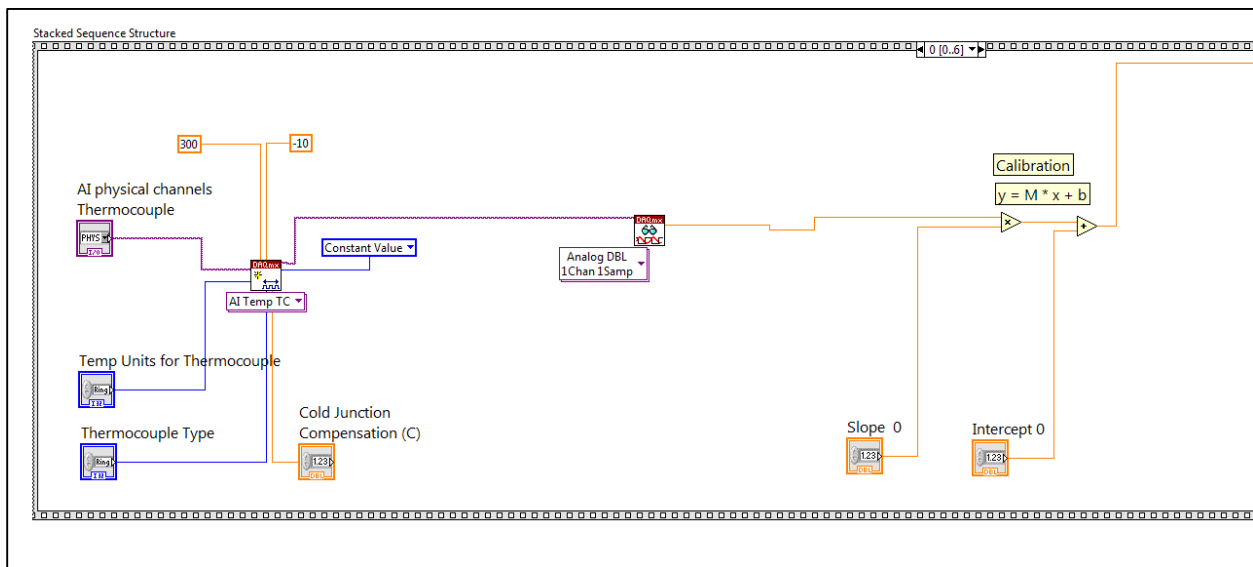


Figure 17: Frame of one stacked sequence gathering data for one thermocouple

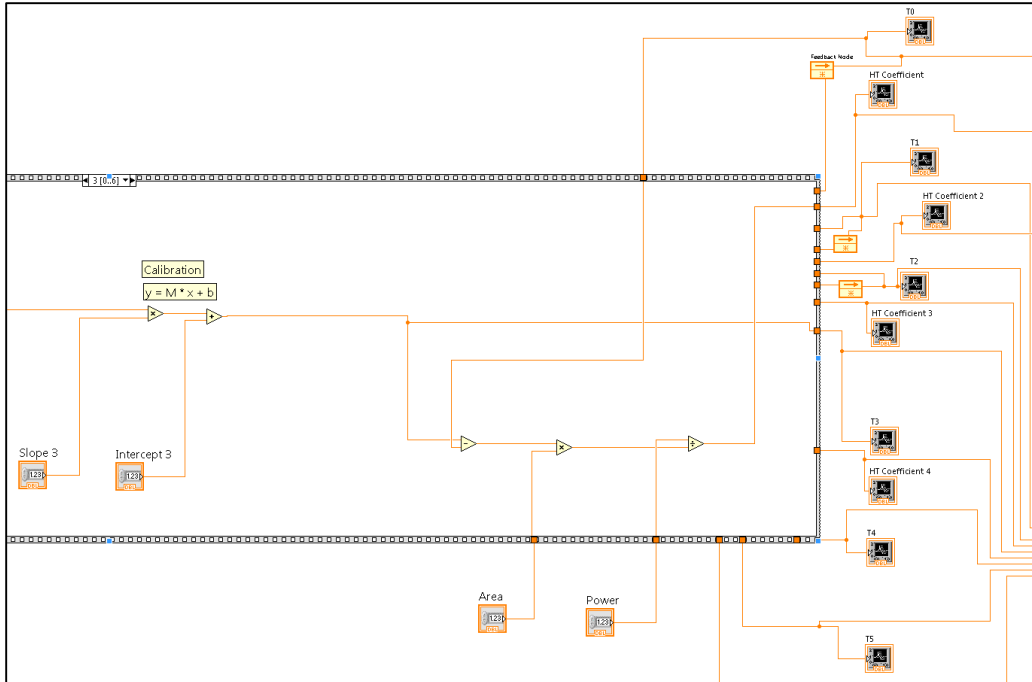


Figure 18: Calculation of the heat transfer coefficient in the LabVIEW program

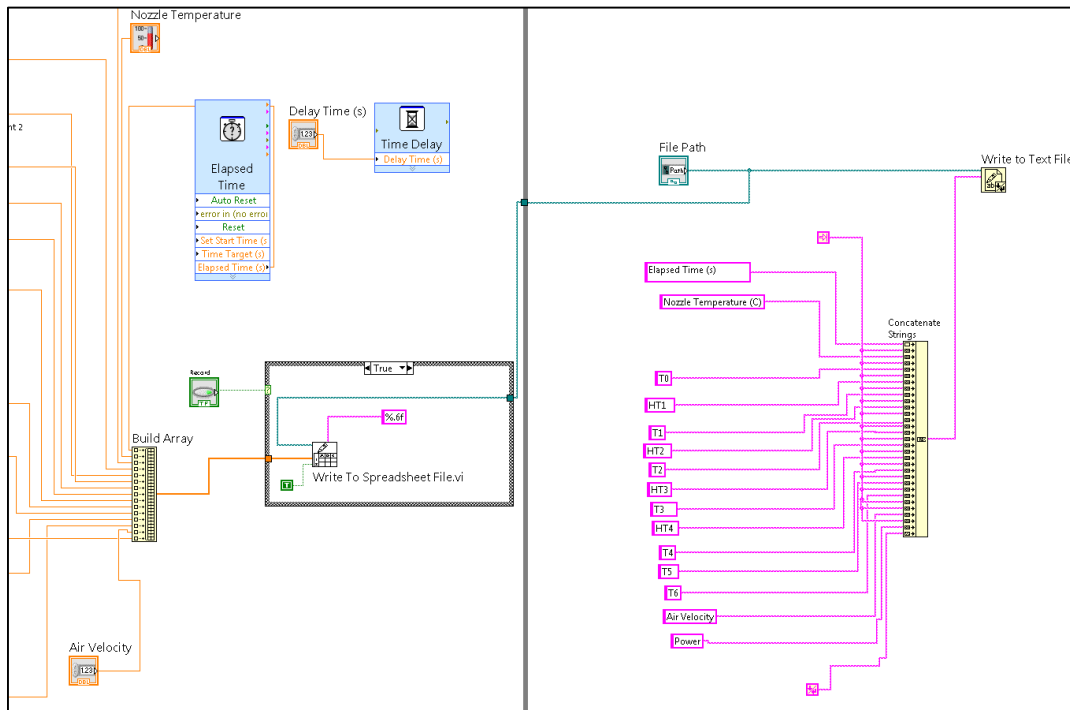


Figure 19: Write-to-file and tab labels on block diagram

For closer view of the front panel of the LabVIEW program and the file while running, please see Appendix C.

### 3.3 Experimentation

In order to analyze the behavior of the convective heat transfer coefficient, a Design of Experiments was created to describe each experiment that our team would conduct. This section will discuss the set up and procedures involved in each of these experiments. The following are an explanation of each operation, a recommendation for future investigation, and an examination of possible sources of error. Appendix B has photos of the instrumentation and setup used to conducted experiments.

#### 3.3.1 Circuit Configuration

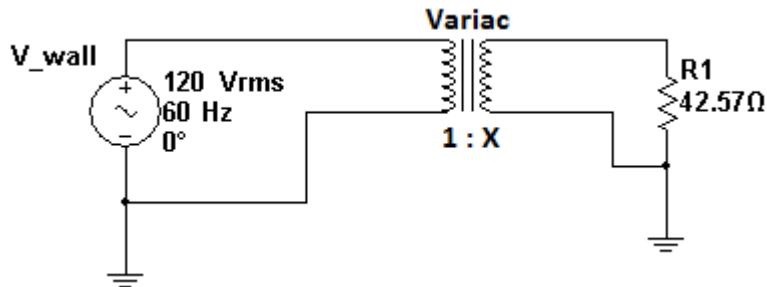


Figure 20: Variac Circuit Configuration

In order to power the heating coil and subsequently heat the test geometry, our team used a variable autotransformer (Variac) with a 3000 Watt capability, illustrated in Figure 20. The Variac was powered by a standard wall socket delivering 120 V<sub>rms</sub> at 60 Hz. Voltage was then controlled by the Variac and sent to the heating coil with a standard 12-gauge cord. To calculate the resistance of the heating coil, the current being delivered to the coil was measured using an Exeter Multimeter. Simple calculation was then completed to obtain the resistance value. This procedure was completed for several high and low voltages, and the resulting resistance values were averaged into the R1 constant 42.57 Ohms. The potential increase in the resistance of the heating coil due to its rise in temperature was neglected in these calculations.

#### 3.3.2 Experimental Procedures

##### 3.3.2.1 Calibration

Before conducting the following experiments, calibration of the thermocouples to the data acquisition box is necessary to obtain accurate measurements. This process will require a

previously calibrated thermocouple and a multimeter. The steps to complete the calibration are as follows:

1. Fasten calibrated thermocouple onto test geometry and connect it to the multimeter.
2. Set variac to 100V and allow the temperature of the test geometry to rise to approximately 250°C.
3. Input correctly measured power into LabVIEW.
4. Once the temperature of the plate has reached steady state, input the temperature reading from the multimeter into LabVIEW.
5. Record approximately 10 data points in LabVIEW at 0 m/s.
6. Using the fan controller, increase the air velocity by .5 m/s.
7. Wait for the plate temperature to reach steady state again and input the temperature reading from the multimeter into LabVIEW.
8. Record approximately 10 data points in LabVIEW.
9. Repeat steps 5-8 until maximum fan speed is reached.
10. Once the tests are completed, stop the program and open the excel file containing the recorded data.
11. Create a scatterplot of the data with Input Temperature on the x-axis and Thermocouple #3 on the y-axis. Add a trend line to the graph and show the equation as well as the  $R^2$  value. Record the slope and intercept of each plot equation.
12. Repeat step 8 for Thermocouple #4, #5, and #6.
13. Plug the slope and intercept of each corresponding thermocouple into the front panel of the LabVIEW program.
14. Be sure to Make Current Values Default under the Edit menu and save the program.

### *3.3.2.2 Air Velocity Test*

After the equipment is calibrated, the air velocity experiment can be conducted. The power and geometric variables will be kept constant for this experiment. The purpose of this test is to observe how the speed of air alone affects the convective heat transfer coefficient. The power will be set at 238 Watts (100V) and the angle of the plate will be set at 0° (flat). The unit should be setup in accordance with the photos in Appendix B. The steps to complete this experiment are as follows:

1. Set variac to 100V.
2. Allow temperature of test geometry to rise to roughly 250°C (approximately 20 minutes).
3. Once the temperature of the plate has reached steady state, set air velocity at 0 m/s and record approximately 10 data points in LabVIEW.
4. Increase the air velocity by .5 m/s using the fan controller and wait for the plate temperature to reach steady state again. Record approximately 10 data points in LabVIEW.
5. Repeat step 4 until the maximum fan speed is reached, leaving the LabVIEW program running continuously during the experiment.

This experiment can be expanded to include data at different power levels and geometric configurations to compare how ‘h’ values are affected. More precise measurements could be taken using smaller incremental increases to improve the accuracy of the experiment.

### *3.3.2.3 Natural Convection Test*

Our device is also capable of measuring the convective heat transfer coefficient for natural convection. To simulate a natural convective environment, air velocity was set to 0 m/s, the geometric configuration remains constant, and the glass top of the test chamber is removed throughout the duration of the experiment. Plate temperature is increased in linear increments by increasing the input Power. The steps to complete this experiment are as follows:

1. To simulate ambient air, remove the top glass from the test chamber.
2. Set the variac to 50V and wait for the temperature of the plate to stabilize.
3. Record approximately 10 data points in the LabVIEW program.
4. Repeat step 2 and 3 for 60V, 70V, 80V, 90V, and 100V.

This experiment can be expanded to include data at different input power levels. More precise measurements could be taken by increasing the number of input voltages at which data points are recorded.

After the data collected in this experiment was analyzed, it was decided that the results were inconclusive. Possible causes of the flawed data were hypothesized when reviewing the experimental procedures. Although the top glass of the test chamber was removed, the side glass pieces remained in place, which could have diminished the authenticity of a naturally convective

environment. The experiment was not conducted in an air tight environment; thus possible external movements of air could have affected the natural convection process. Conjecture was also made that the instrumentation used, specifically the thermocouples, may not have been correctly calibrated for this experiment, or were not functioning properly during the test. In future experiments, it is the recommendation of this team that stricter measures be taken to simulate a naturally convective climate, and the thermocouples be recalibrated and tested before the experiment is conducted.

#### *3.3.2.4 Geometry Orientation Test*

The geometric configuration tests were completed in a similar fashion to the air velocity tests. At each geometric configuration, the plate was heated to roughly 250°C and air was drawn through the test chamber at increasing velocities. The test geometry used in this experiment was mounted to an adjustable base stand so that the angle of the plate could be increased. The steps to complete this experiment are as follows:

##### **0° Plate Angle**

1. Remove the top of the test chamber and set the test plate's angle at 0° to the bottom of test chamber. The plate should be in its resting, flat position.
2. Replace the glass top of the test chamber, and ensure a good seal is made between the silicon and the glass.
3. Set the variac at 100V and allow the temperature of the test geometry to rise to roughly 250°C (approximately 20 minutes).
4. Once the temperature of the plate has reached steady state, set air velocity at 0 m/s. Record approximately 10 data points in LabVIEW.
5. Record approximately 10 data points in LabVIEW at 0 m/s.
6. Using the fan controller, increase the air velocity by .5 m/s.
7. Wait for the plate temperature to reach steady state again and input the temperature reading from the multimeter into LabVIEW.
8. Record approximately 10 data points in LabVIEW.
9. Repeat steps 5-8 until maximum fan speed is reached, leaving the LabVIEW program running continuously during the experiment.

## 15° Plate Angle

1. Remove the top of the test chamber and set the test plate's angle at 15° to the bottom of test chamber, shown in Figure 21. The plate should be in its resting, flat position.

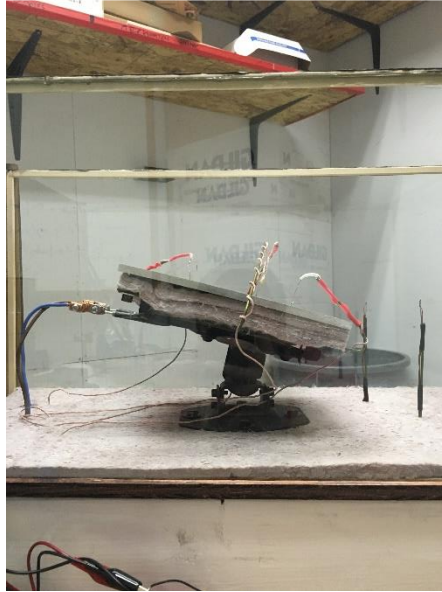


*Figure 21: 15 Degree Orientation Angle*

2. Replace the glass top of the test chamber, and ensure a good seal is made between the silicon and the glass.
3. Set the variac at 100V and allow the temperature of the test geometry to rise to roughly 250°C (approximately 20 minutes).
4. Once the temperature of the plate has reached steady state, set air velocity at 0 m/s. Record approximately 10 data points in LabVIEW.
5. Record approximately 10 data points in LabVIEW at 0 m/s.
6. Using the fan controller, increase the air velocity by .5 m/s.
7. Wait for the plate temperature to reach steady state again and input the temperature reading from the multimeter into LabVIEW.
8. Record approximately 10 data points in LabVIEW.
9. Repeat steps 5-8 until maximum fan speed is reached, leaving the LabVIEW program running continuously during the experiment.

### 30° Plate Angle

1. Remove the top of the test chamber and set the test plate's angle at 30° to the bottom of test chamber, shown in Figure 22. The plate should be in its resting, flat position.



*Figure 22: 30 Degree Orientation Angle*

2. Replace the glass top of the test chamber, and ensure a good seal is made between the silicon and the glass.
3. Set the variac at 100V and allow the temperature of the test geometry to rise to roughly 250°C (approximately 20 minutes).
4. Once the temperature of the plate has reached steady state, set air velocity at 0 m/s. Record approximately 10 data points in LabVIEW.
5. Record approximately 10 data points in LabVIEW at 0 m/s.
6. Using the fan controller, increase the air velocity by .5 m/s.
7. Wait for the plate temperature to reach steady state again and input the temperature reading from the multimeter into LabVIEW.
8. Record approximately 10 data points in LabVIEW.
9. Repeat steps 5-8 until maximum fan speed is reached, leaving the LabVIEW program running continuously during the experiment.

This experiment has many opportunities for expansion. This experiment could be conducted again at different Power levels to observe the rate at which the 'h' value changes at higher

and lower temperatures. The current base mount is only adjustable up to  $30^\circ$ . In future experiments, a different mounting mechanism could allow a fuller range of motion so that all angles through  $90^\circ$  could be tested. Cylindrical, spherical and prismatic geometries could also be configured into this device and tested at different geometric orientations.

#### *3.3.2.5 Textbook Sample Problem*

Problems such as the one shown in Figure 27 could be actively demonstrated in class. After theoretical calculation is performed, students can compare their calculated values to the ones obtained through experimentation using this device. Please reference Appendix G for a detailed sample problem that can be tested using the demonstration unit.

## Chapter 4: Results and Analysis

The following section will outline the results from numerous data collection experiments conducted using the heat transfer demonstration unit constructed by our team. Comparisons between MATLAB predictions and experiment results are shown and discussed in the following section. Additional graphs, charts, and discussion can be found in Appendix D and Appendix E.

### 4.1 MATLAB Prediction and Experimental Result for $\Delta T$ vs. Power

Figure 23 shows one of the predictions done at the early stages of this project. It explicitly depicts the linear relationship between the temperature differential,  $\Delta T$ , and power. The slope comes from the equation,  $\dot{Q} = hA\Delta T$ , where the heat transfer coefficient and the area of the plate, determine that slope. Since this experiment was done with wind blown over the plate, the heat transfer equation for forced convection and laminar flow was implemented. Further, since the Prandtl number for air at room temperature is 0.713, the equation for the average Nusselt number was:  $\overline{Nu} = 0.664\sqrt{Re} * \sqrt[3]{Pr}$

Here,  $Re$  stands for the Reynold's number. The Reynold's number is defined by:  $Re = \frac{v*D}{\nu}$ . Here,  $v$  is the velocity,  $D$  is the hydraulic diameter,  $\nu$  is the kinematic viscosity. Finally,  $h$  is defined by:  $h = k \frac{\overline{Nu}}{L}$ , where  $k$  is thermal conductivity of air,  $\overline{Nu}$  is the average Nusselt number on the plate. Once all of the values were determine, the air velocity was set from 0.5 to 4 m/s in increments of 0.5 m/s in order to define 8 distinct plots. Figure 23 also shows a dashed line at fixed power. That line represents the maximum power that could be reached in this project's setup.  $\Delta T$  was set as the independent variable linearly growing from 0 to 450 K.

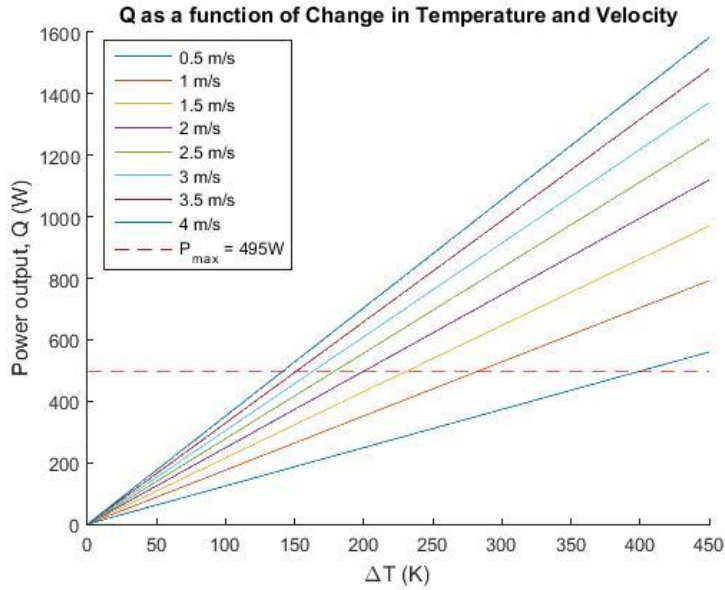


Figure 23: Predicted  $Q$  as a Function of  $\Delta T$  and Air Velocity

Figure 24 depicts our experimental results. The data can be seen at five different power levels with the points spread out. It is clear that by comparing the two plots, the slopes for the predicted values were higher and lines were better defined. This resulted in the measurement of lower convective heat transfer coefficients. Yet, the correlation that higher air velocities represent higher values of 'h' is still accurate.

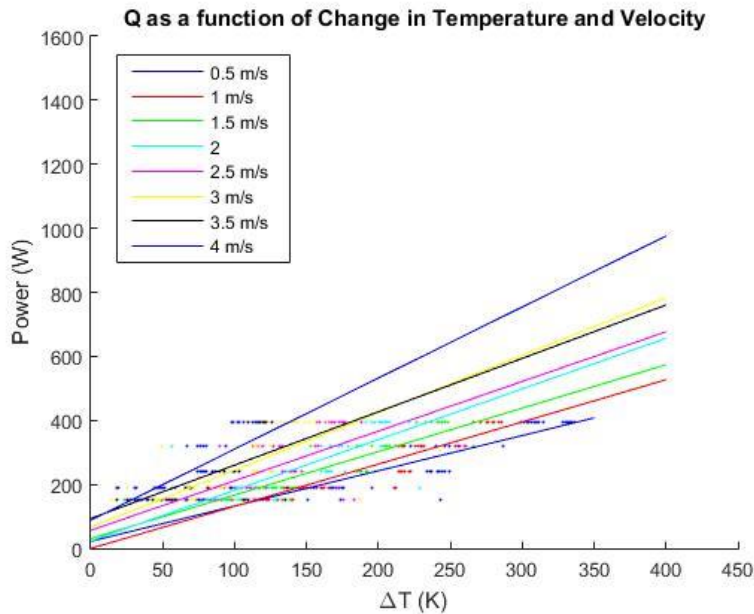


Figure 24: Experiment Results:  $Q$  as a Function of  $\Delta T$  and Air Velocity

## 4.2 MATLAB Prediction vs. Experimental Data

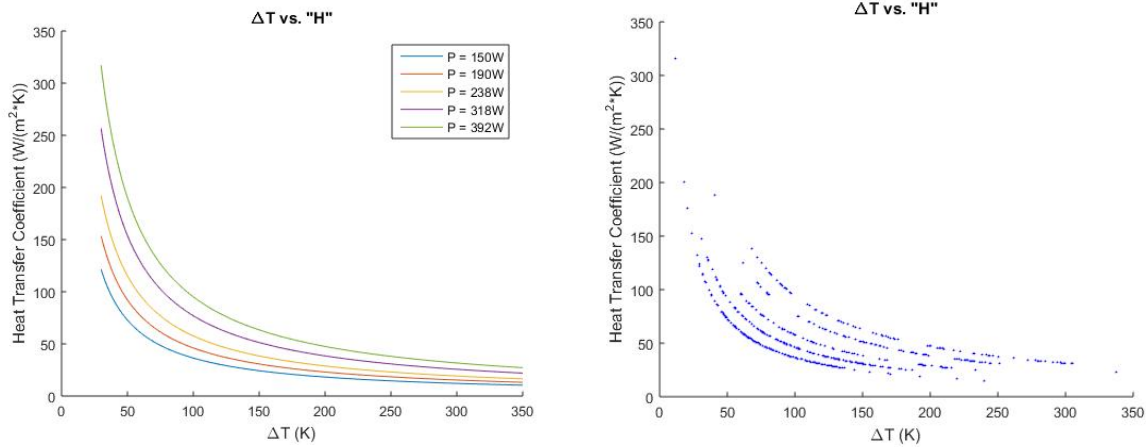


Figure 25: At left, predicted  $\Delta T$  vs. 'h'. At right, Experimental data  $\Delta T$  vs. 'h'.

Figure 25 left was generated through a MATLAB script. It is the prediction for a correlation between the convective heat transfer coefficient and the temperature differential. The five separate curves correspond to five different power inputs at 150W, 190W, 238W, 318W and 392W. These values correspond to the ones in Figure 25 right, which represents the results from experiments of different air velocities. These two plots were calculated separately, but they clearly represent the same curves and equation,  $\dot{Q} = hA\Delta T$ . Thus, Figure 26 superimposes both plots. It is clear that the experimental data is spot on the predicted plots. This serves as proof the LabVIEW program is correct and has used the right equation to determine the heat transfer coefficient.

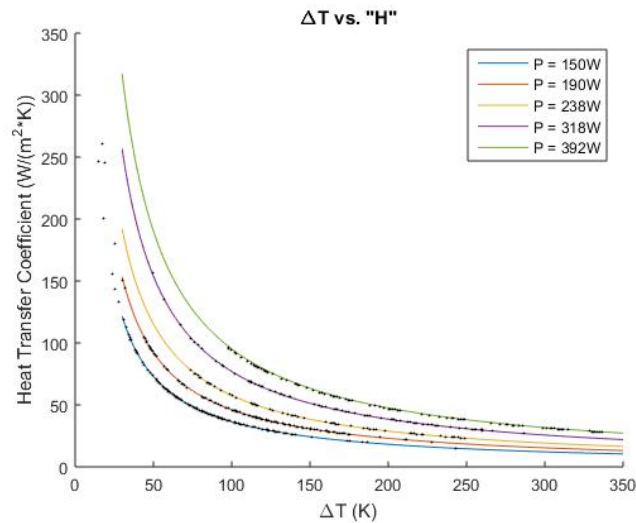


Figure 26: Experimental data  $\Delta T$  vs. 'h' superimposed onto predicted  $\Delta T$  vs. 'h'

### 4.3 Plate Orientation Angle Experiment

A significant experiment conducted by our team included testing for the heat transfer coefficient at different plate orientation angles. The tests included ‘h’ measurements at 0, 15, and 30 degrees of elevation while varying air velocity over the plate, reference chapter 3 for more information about the test procedure. Figure 27 displays the results of orientation testing. The heat transfer coefficient is shown to increase with increasing plate orientation angles; therefore, the highest values of ‘h’ are seen to occur with steeper geometric orientations. It can be seen that higher values of ‘h’ translate to higher rates of heat transfer. This is because, at a constant heat flux, changes in temperature must be smaller to accommodate large ‘h’ values. Thus, surface temperature of the test configuration is more comparable to that of the configuration’s surroundings when higher ‘h’ values are present. Figure 27 presents data from thermocouple number four on the unit, and the graphs from the other thermocouples can be found in Appendix E.

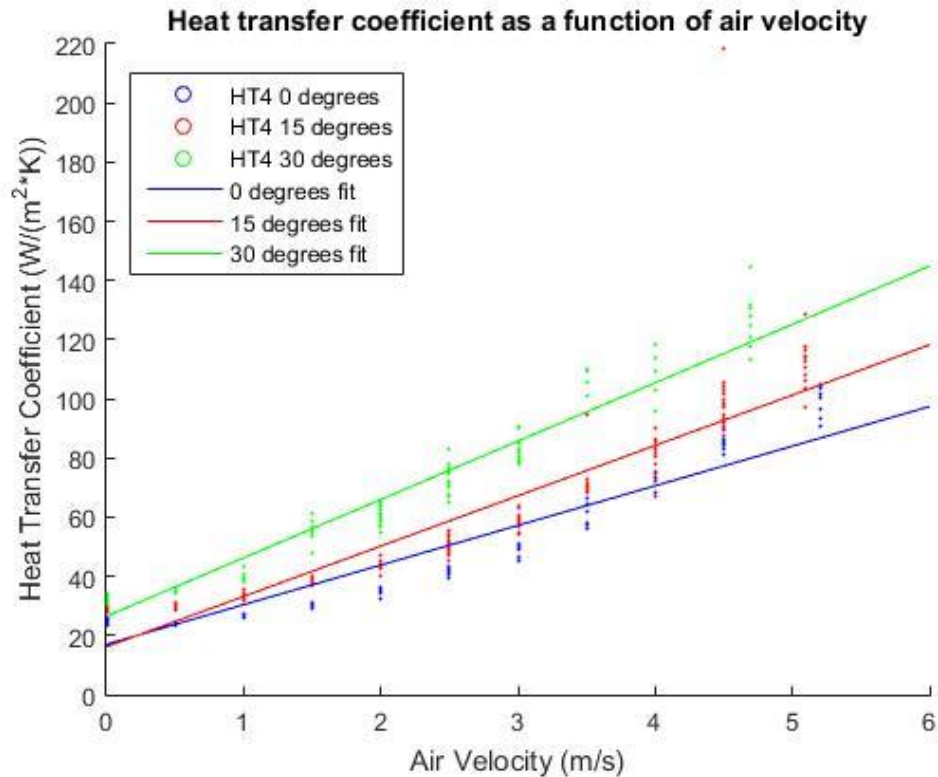


Figure 27: 'h' as a Function of Air Velocity

#### 4.4 Power vs. Heat Transfer Coefficient Experiment

Figure 28, displays the heat transfer coefficient as a function of air velocity and power. The goal of the experiment was to determine the relationship between 'h' and the power input into the test. Since all curves are intertwined, power does not affect the heat transfer coefficient. There is not an increasing or decreasing correlation between input power and the determination of 'h'. The input power directly influences the surface temperature of plate, thus proving the increasing surface temperature does not influence the heat transfer coefficient, assuming other variables remain constant between power experiments.

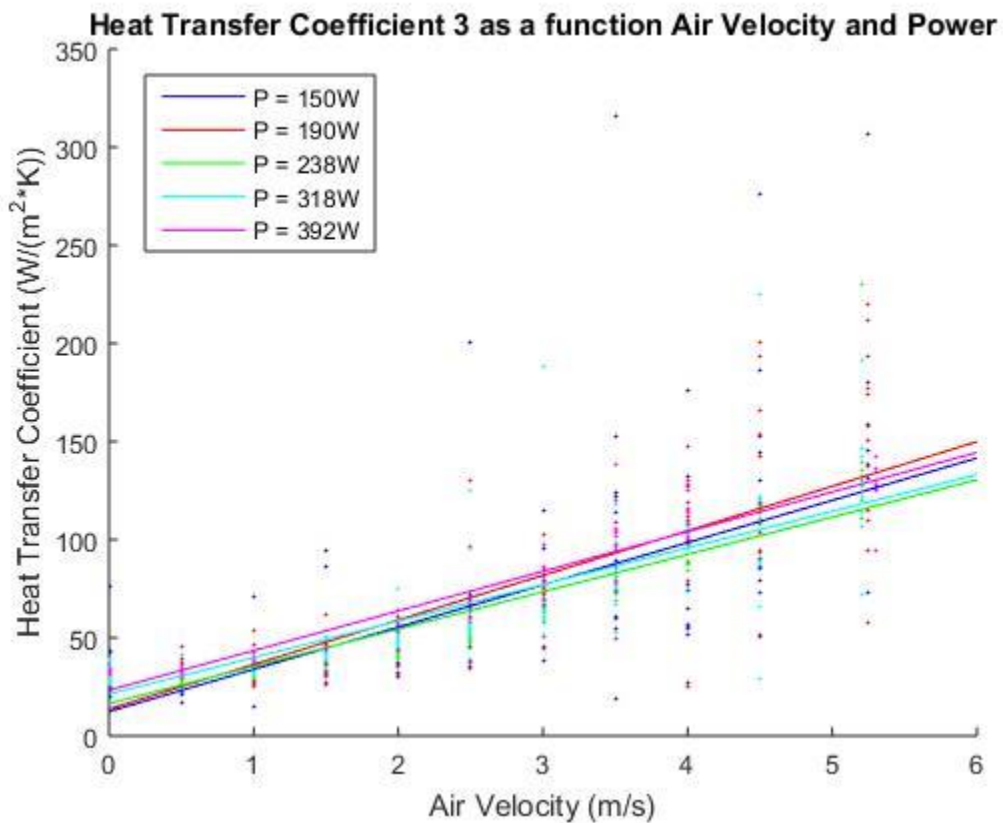


Figure 28: 'h' as a Function of Air Velocity and Power

## 4.5 General Heat Transfer Coefficient Experiment Data

The following determine our experimental for different power inputs and air velocities. All of these values correspond to the average of all data points collected. This table can be used a reference in our project.

Table 2: General 'h' Coefficients for Air Velocity and Power

HT3 [W/ (K*m <sup>2</sup> )]	Power [W]	Air Velocity [m/s]									
		0	0.5	1	1.5	2	2.5	3	3.5	4	4.5
	150.3	29.7	26.3	30.4	41.9	44.0	58.3	67.2	98.9	84.2	125.1
	190.3	29.9	32.0	34.0	38.6	47.4	63.3	68.0	79.9	105.0	125.4
	238.0	28.1	27.0	29.6	35.3	41.6	50.2	61.5	75.2	89.5	112.9
	317.8	32.8	33.0	34.8	42.2	51.7	64.9	82.2	82.4	97.0	107.5
	392.7	33.0	32.8	39.4	45.6	55.6	67.3	81.4	103.0	114.2	N/A

HT4 [W/ (K*m <sup>2</sup> )]	Power [W]	Air Velocity [m/s]									
		0	0.5	1	1.5	2	2.5	3	3.5	4	4.5
	150.3	31.1	31.2	30.9	45.8	41.5	48.3	71.0	80.1	83.9	115.7
	190.3	28.9	31.9	33.2	38.6	41.8	48.7	65.0	88.3	114.5	125.3
	238.0	24.7	23.9	26.6	30.4	34.7	41.3	49.5	60.1	72.1	85.1
	317.8	36.7	32.4	33.9	39.5	52.1	60.7	79.0	77.9	99.2	123.1
	392.7	28.3	29.5	33.9	39.1	46.8	55.4	65.9	78.7	89.7	N/A

HT5 [W/ (K*m <sup>2</sup> )]	Power [W]	Air Velocity [m/s]									
		0	0.5	1	1.5	2	2.5	3	3.5	4	4.5
	150.3	26.4	28.3	32.0	40.2	43.0	65.1	73.4	71.8	89.5	88.6
	190.3	28.1	32.3	35.3	39.7	49.2	67.0	62.4	115.0	89.1	125.8
	238.0	25.8	28.0	28.9	34.0	39.4	47.1	57.6	68.9	89.8	119.8
	317.8	29.0	29.6	32.3	39.8	44.3	58.8	82.3	78.7	83.1	108.3
	392.7	29.0	31.9	37.6	44.1	53.7	64.8	78.9	96.8	106.9	N/A

HT6 [W/ (K*m <sup>2</sup> )]	Power [W]	Air Velocity [m/s]									
		0	0.5	1	1.5	2	2.5	3	3.5	4	4.5
	150.3	25.7	32.2	30.9	41.6	49.5	54.9	66.5	89.9	93.5	112.6
	190.3	25.6	33.2	36.6	39.3	51.2	57.4	82.7	79.9	129.6	131.6
	238.0	27.4	32.6	36.4	40.0	47.5	56.4	70.2	82.0	99.2	113.0
	317.8	30.8	34.0	41.0	41.8	45.9	52.0	61.1	82.2	98.8	107.0
	392.7	30.9	35.3	41.7	48.0	58.8	66.8	85.6	97.8	112.9	N/A

## 4.6 Possible Sources of Experimental Error

One possible source of error could be the measurements from the DAQ box. As mentioned in the Instrumentation section, the DAQ box has a resolution of approximately  $305\mu\text{V/bit}$ . This seems like a high resolution for many instruments. However, voltage differentials produced by thermocouples are very small in the order of tens of millivolts per degree Celsius. In fact, on the National Instruments website, one can find the voltage output, in millivolts, of K-type thermocouples for various temperatures. Since in this project we are not dealing with temperatures lower than  $0^\circ\text{C}$  and higher than  $400^\circ\text{C}$ , the linear resolution for this type of thermocouple would be  $\frac{16.397\text{mV}-0\text{mV}}{400^\circ\text{C}-0^\circ\text{C}} = 40.993 \frac{\mu\text{V}}{^\circ\text{C}}$ .  $16.397\text{mV}$  represents the output voltage differential at  $400^\circ\text{C}$  and  $0\text{mV}$ , at  $0^\circ\text{C}$ . Comparing the resolution of the DAQ Box to that of the thermocouple would lead to  $\frac{305 \frac{\mu\text{V}}{\text{bit}}}{40.993 \frac{\mu\text{V}}{^\circ\text{C}}} = 7.44 \frac{^\circ\text{C}}{\text{bit}}$ . Finally, this means that every bit in the DAQ Box would only measure differences in quantities of  $7.44^\circ\text{C}$  for K-type thermocouples. This lack of accurate measurements could be a source of error in the data.

During the construction of this device, thermocouples were pushed through a small from the bottom of the wind tunnel into the test chamber. This could have damaged the metal wires that create the small voltage differentials. Also, the thermocouples were positioned such that the welded ball touches the hot plate. Yet, high temperature thermal pastes could glue the thermocouples to the plate and provide better readings for the thermocouples. Further, due to their placement, thermocouples are not insulated from air. This could cause the wires of the thermocouple to act as a heat sink, consequently leading to bad readings from the thermocouples.

## Chapter 5: Conclusion and Recommendations

After design, construction, and experimentation of our project, the demonstration device is now capable of measuring the convective heat transfer coefficient 'h'. Due to its portability it can be easily set up and used in a classroom as a visual aid. Our team's attention to detail and professional level of craftsmanship has made the device a reliable source of data acquisition that will remain functional for years to come. Through our team's own design of experiments, we began investigating the relationship between the geometry, air flow, and the convective heat transfer coefficient.

As predicted in Chapter 3, the faster air is blown across the test geometry the more heat will be transferred between the two mediums, and thus, the cooler the plate will become. And because higher rates of heat transfer correspond to higher values of 'h', it follows that as air velocity increases, 'h' also increases. Figure 24 shows the linear correlation between the air velocity and the temperature of the plate.

From the results our team collected, a relationship between the convective heat transfer coefficient and geometric orientation can be interpreted. The analysis of gathered data determined that steeper slopes in the test geometry correspond to higher rates of heat transfer and thusly higher values of 'h'. In future experiments, different mounting mechanisms could allow a fuller range of motion so that all angles through 90° could be tested. Cylindrical, spherical and prismatic geometries could also be mounted into this device and tested at different geometric orientations.

## References

- Awuah, G. B., Ramaswamy, H. S., & Simpson, B. K. (1995). Comparison of two methods for evaluating fluid-to-surface heat transfer coefficients. *Food Research International*, 28(3), 261-271. Retrieved November 23, 2015.
- Baals, Donald D., and William R. Corliss. Wind Tunnels of NASA. Washington, D.C.: Scientific and Technical Information Branch, National Aeronautics and Space Administration, 1981. Print.
- Bergman, T. L., Lavine, A. S., Incropera, F. P., & Dewitt, D. P. (2007). *Fundamentals of Heat and Mass Transfer* (7th ed.). Hoboken, NJ: John Wiley.
- Bonwell, C. C., & Eison, J. A. (1991). *Active Learning: Creating Excitement in the Classroom* (Rep. No. ED 336 049). Washington, DC: ERIC Clearinghouse on Higher Education. doi:ASHE-ERIC Higher Education Report. U.S. Department of Education
- CDC/NIOSH. *Noise and Hearing Loss Prevention*. Cincinnati, OH: U.S. Department of Health and Human Services; 1998.
- Cuesta, F. J., Lamúa, M., & Alique, R. (2012). A new exact numerical series for the determination of the Biot number: Application for the inverse estimation of the surface heat transfer coefficient in food processing. *International Journal of Heat and Mass Transfer*, 55(15-16), 4053-4062. doi:10.1016/j.ijheatmasstransfer.2012.03.047
- Dunbar, Brian. "What Are Wind Tunnels?" NASA. NASA, 24 June 2014. Web.
- Fokaides, P. A., & Kalogirou, S. A. (2011). Application of infrared thermography for the determination of the overall heat transfer coefficient (U-Value) in building envelopes. *Applied Energy*, 88(12), 4358-4365. doi:10.1016/j.apenergy.2011.05.014
- Gallagher, J. E. (2005, May 11). The Effects of Flow Conditioning. Retrieved February 24, 2016, from <http://www.wwdmag.com/flow-metering/effects-flow-conditioning>
- Guo, Z., Xiong, S., Liu, B. C., Li, M., & Allison, J. (2009). Determination of the metal/die interfacial heat transfer coefficient and its application in evaluating the pressure distribution inside the casting during the high pressure die casting process. *International Journal of Cast Metals Research*, 22(1-4), 327-330. doi:10.1179/136404609x368109
- Hake, R. R. (1998). Interactive-engagement versus traditional methods: A six-thousand-student survey of mechanics test data for introductory physics courses. *Am. J. Phys. American Journal of Physics*, 66(1), 64. doi:10.1119/1.18809
- Kirby, Mark S., and John Hansman. "EXPERIMENTAL MEASUREMENTS OF HEAT TRANSFER FROM AN ICED SURFACE DURING ARTIFICIAL AND NATURAL CLOUD ICING CONDITIONS." (n.d.): n. pag. NASA.gov. Web.

Metha R. D., Bradshaw P. "Design Rules for Small Low Speed Wind Tunnels" Journal of Royal Aeronautical Society 1979, Vol. 73

Pate, M. B. (2008). An active learning approach for teaching undergraduate heat transfer. In *2008 Proceedings of the ASME Summer Heat Transfer Conference* (Vol. 3, pp. 677-683). ASME.

Patil, Pranit M., Amol P. Yadav, and P. A. Patil, Dr. "Comparative Study between Heat Transfer through Laminar Flow and Turbulent Flow." *International Journal of Innovative Research in Science, Engineering and Technology* 4.4 (2015): n. pag. Web.

Suh, Nam P. *The Principles of Design*. New York: Oxford UP, 1990. Print.

Tables of Thermoelectric Voltages for All Thermocouple Types. (n.d.). Retrieved April 20, 2016, from <http://www.ni.com/white-paper/4231/en/#toc2>

Tan, F. L., & Fok, S. C. (2008). Development of interactive learning activities in heat transfer. *World Review of Science, Technology and Sustainable Development*, 5(3-4), 354-372. Retrieved January 14, 2016.

"Thermal Wind Tunnel." Audi Wind Tunnels AUDI AG. N.p., n.d. Web. Kumar, A., and N. Barthakur. "Convective Heat Transfer Measurements of Plants in a Wind Tunnel." *Springer Link*. Kluwer Academic Publishers, Dec. 1971.

## Appendix A: Construction

The construction process began with the purchase of all required material through internet purchases and trips to local hardware stores. The following outline shows the steps our team took to construct a stable and elegant wind tunnel on a strict budget.

### 1. Construct Diffuser

- a. Cut plywood to size and glue + screw together using angle brackets



### 2. Construct Nozzle

- a. Cut plywood to size and glue + screw together using angle brackets



### 3. Construct Support Beams

- a. Cut 2x4x8 to account for the slope of the nozzle and diffuser



4. Assemble Subcomponents

- a. Attach diffuser, nozzle and base plate to the horizontal support beams



5. Attach Glass

- a. Fix the glass panels to the base grooves using clear epoxy



6. Attach Fan Unit

- a. Cut circular hole in square plywood section. Glue the fan within the circle and affix that subunit to the diffuser.



7. Honeycomb Installation

- a. We used 3M foam double-sided type to restrain the honeycomb within the nozzle.



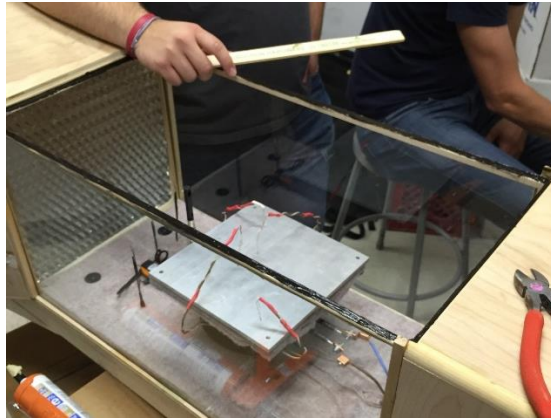
8. Screen Application

- a. Apply a screen to the nozzle to prevent foreign object suction.
- b. Apply metallic screen to the diffuser to prevent hand injury – a “requirement” of Torbjorn Bergstrom, PhD Pursuant.



9. Apply Silicon

- a. Apply silicon to the top of the glass panels to ensure proper seal



10. Stand and Staining

- a. Prepare wood by sanding out imperfections, then apply stain and polyurethane.

11. Begin testing!

## Appendix B: Instrumentation and Unit Setup



Infrared Laser Thermometer



Fan Unit Controller



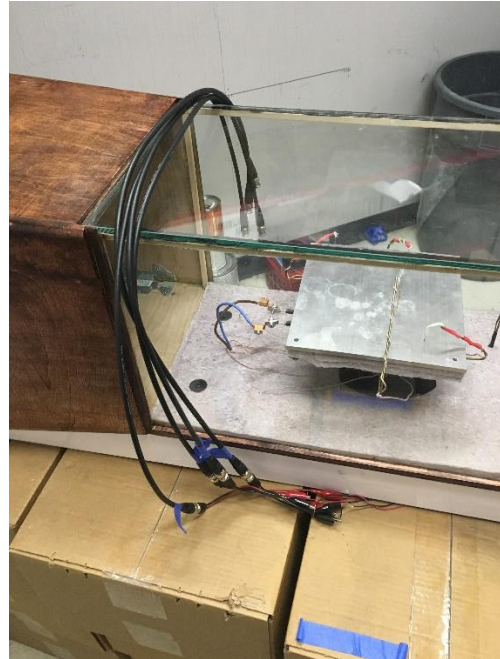
Hot Wire Anemometer



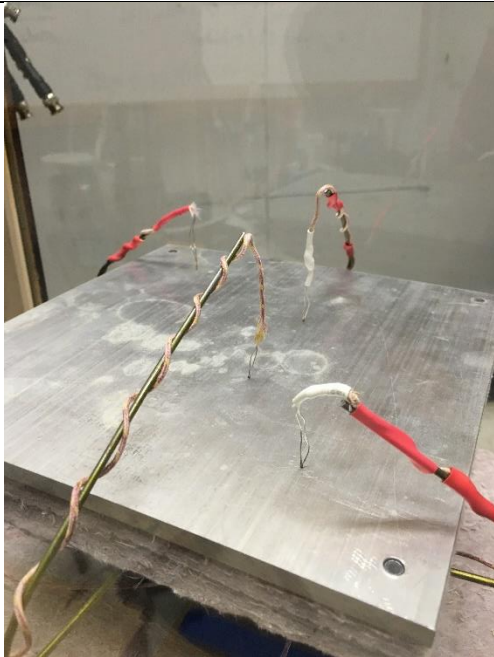
Hot Wire Anemometer



Data Acquisition Box (DAQ)



BNC Cables



Type K Thermocouple



Type T Thermocouple



Thermocouple Cold Junction



Cold Junction Demonstration



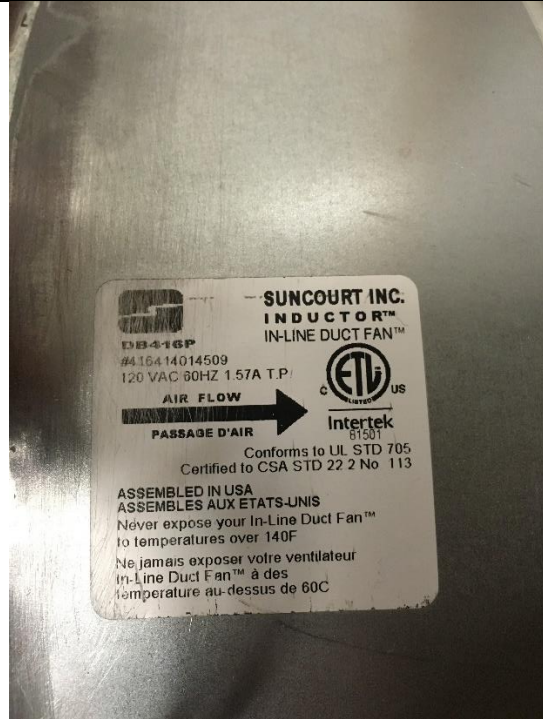
Variac



Suction Cup Handle



Fan



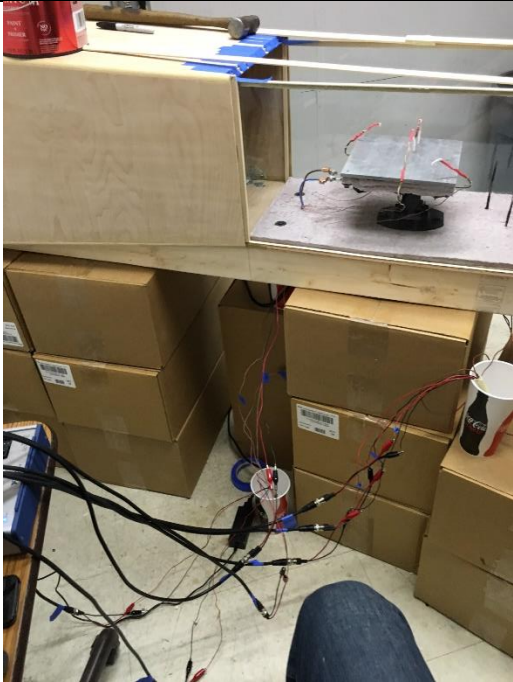
Fan Specifications



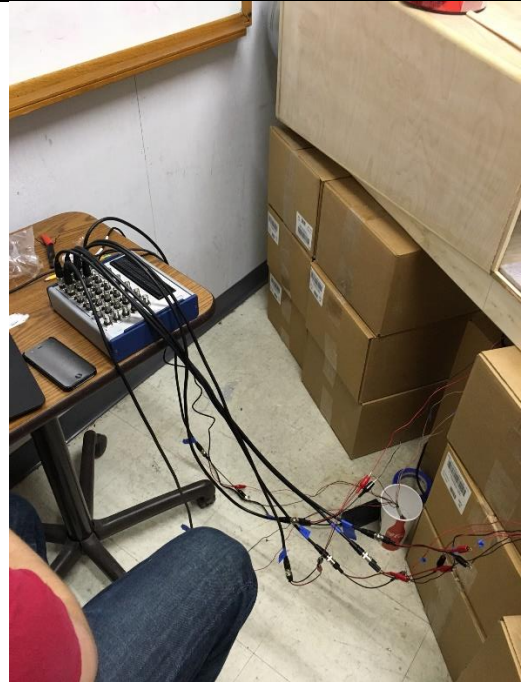
Honeycomb



Silicon



BNC Connections for setup



BNC Connections for setup



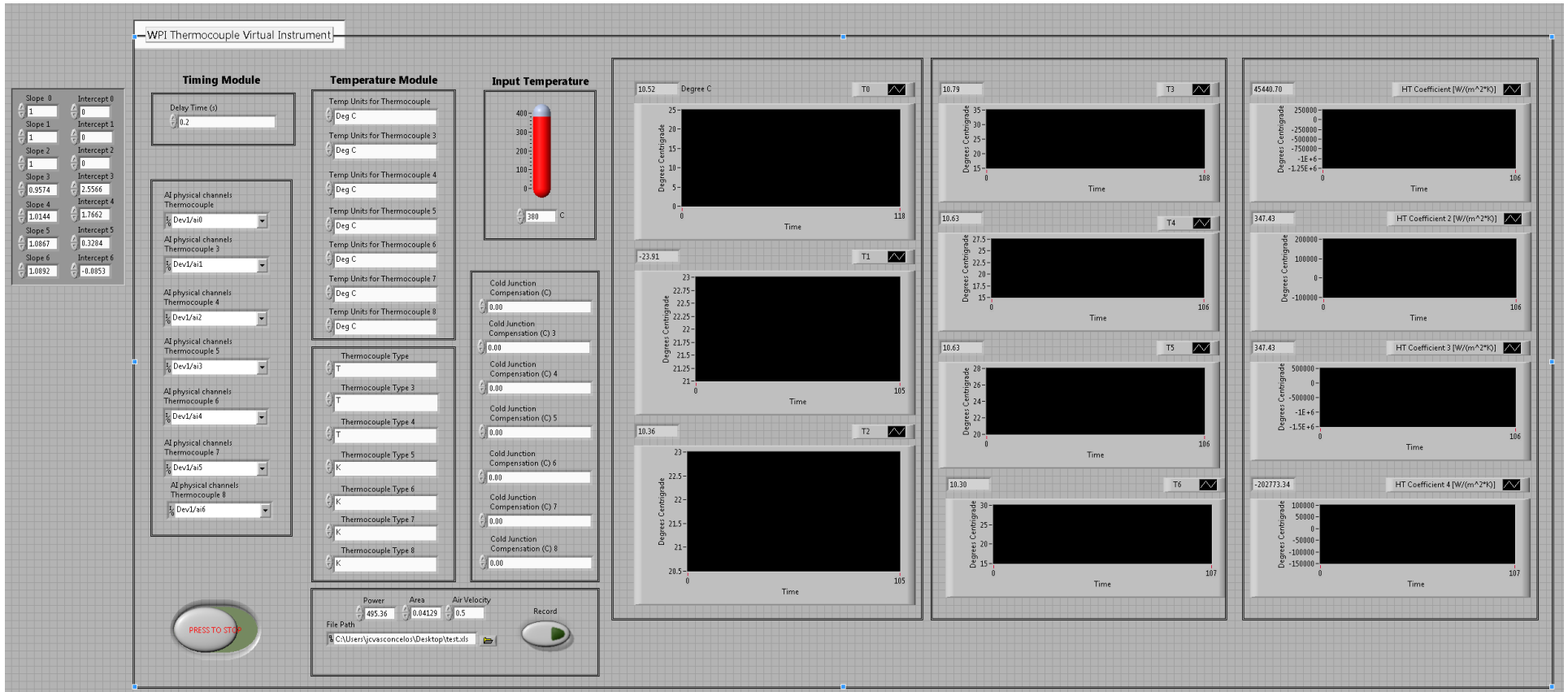
Complete Setup

## Complete Demonstration Unit Set-up

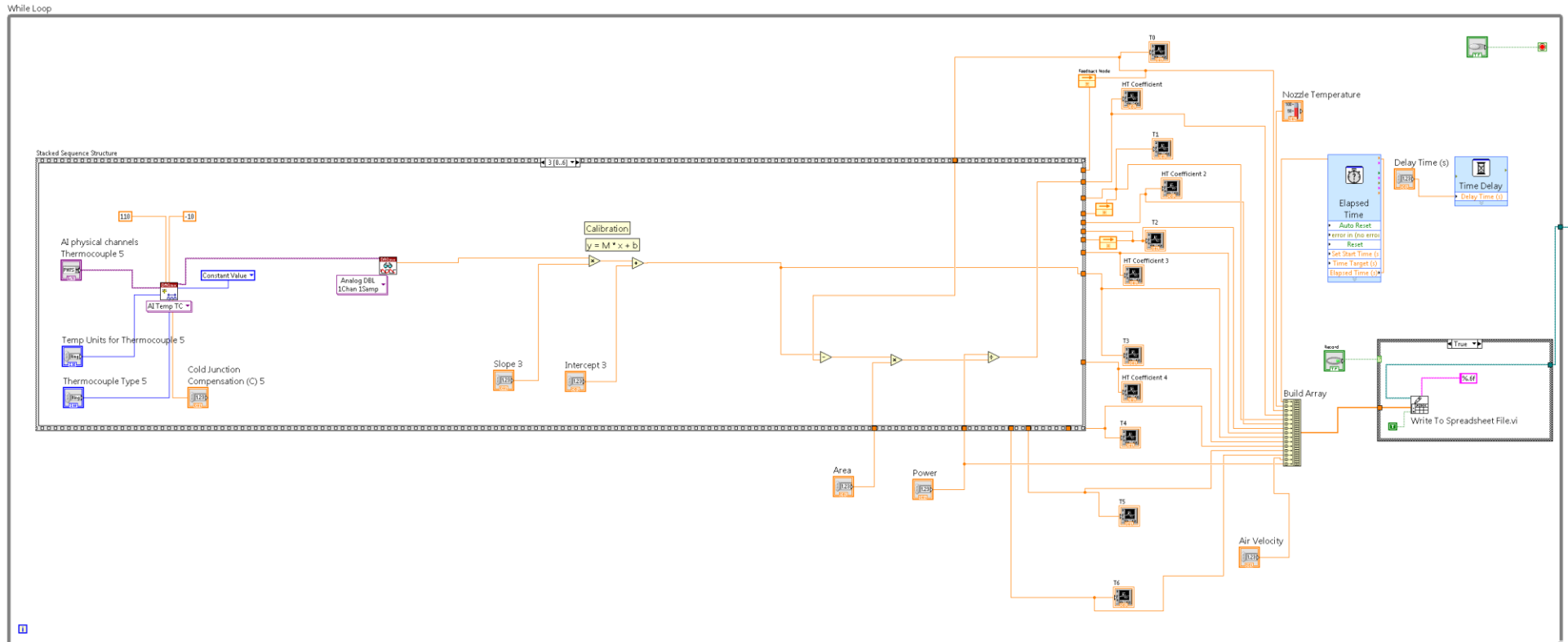
1. Move Demonstration Unit to Classroom
2. Ensure you have the following equipment (Photos Above)
  - a. DAQ BOX
  - b. BNC Cables attached to correct Thermocouples (Labeled 0-6)
  - c. Laptop Computer with LabVIEW and Specific Program
  - d. Cups
  - e. ICE
  - f. Extension Cords for Fan, Variac, DAQ Box, and Laptop
  - g. Hot Wire Anemometer
  - h. Fan Speed Controller
3. Fill cups with ice and water
4. Place three thermocouple cold junctions into cups of ice-water
5. Connect BNC Cables to DAQ Box
  - a. Connect across the top most row Thermocouples 0,1,2,3
  - b. Connect across the second row from top Thermocouples 4,5,6
6. Connect DAQ Box to power source and ensure power switch is on
7. Connect DAQ Box to Computer
8. Open LabVIEW Program on Computer
9. Connect RED Banana Plug from Power cord to RED Input Slot on Variac
10. Connect BLACK Banana Plug from Power cord to BLACK Input Slot on Variac
11. Connect RED Banana Plug from Demonstration Device to RED Output Slot on Variac
12. Connect BLACK Banana Plug from Demo Device to BLACK Output Slot on Variac
13. Ensure Variac power switch is off and voltage set to ZERO
14. Connect Power Cord to outlet
15. Ensure Fan Speed Controller is in off position
16. Connect Fan Speed Controller to fan and then to extension cord and then to outlet
17. Connect Hot Wire Anemometer (HWA) to Phone
18. Place HWA inside test section
19. Begin running the LabVIEW program by pushing the white arrow in top left
  - a. Do not hit button that says run program continuously
20. Please refer to Section 3.3 for step-by-step directions for running experiments
21. Set Variac to desired voltage and turn on power switch
22. Have Fun and Be Safe!

## Appendix C: LabVIEW Program

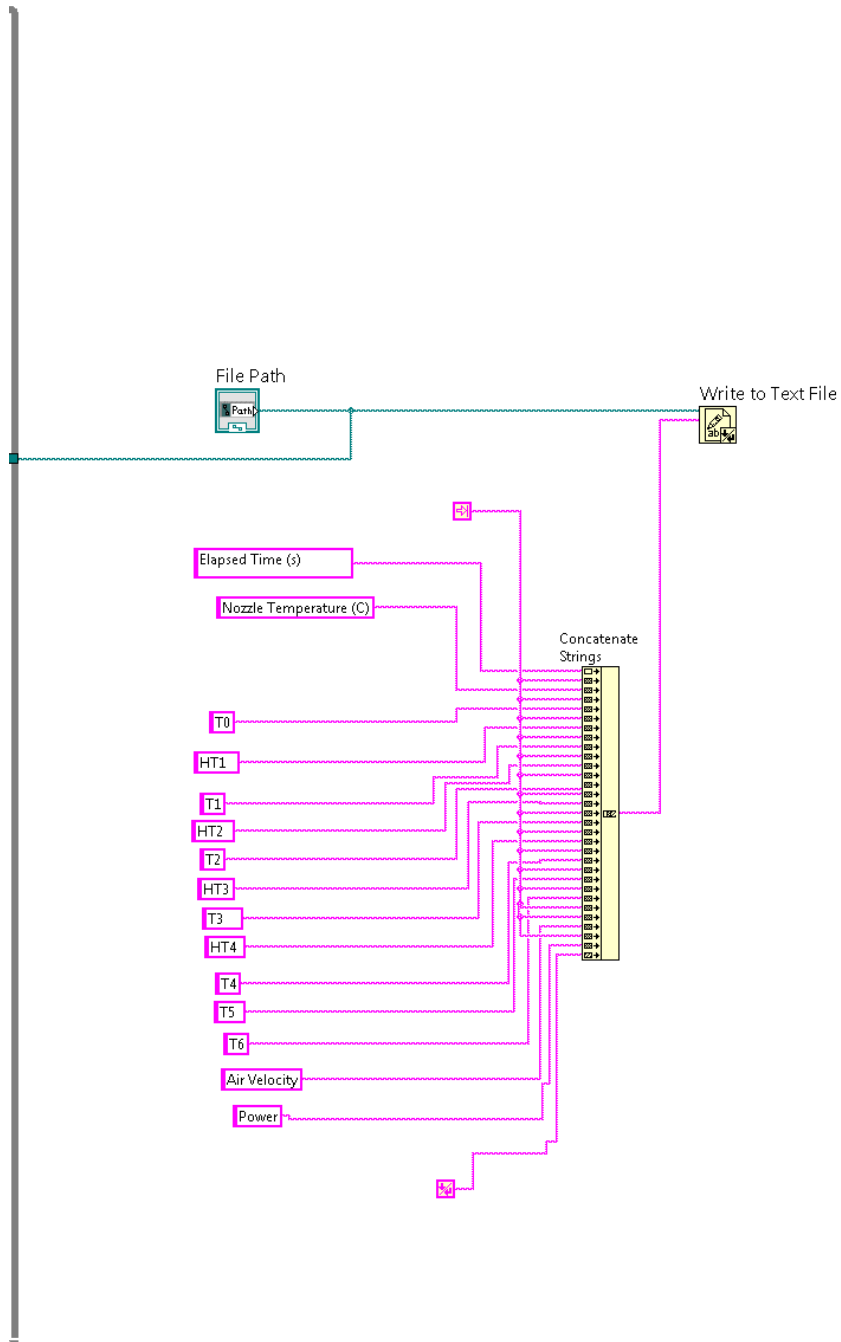
LabVIEW Front Panel: Elements on the left side of the screen represent the parameters that are adjusted for tests; on the right, the charts represent the measurements of the thermocouples, as well as calculated heat transfer coefficients.



LabVIEW Block Diagram 1: This represents the processing parts of the LabVIEW program. They are all inside a while loop that continuously runs thermocouple measurements and calculates the heat transfer coefficient.



LabVIEW Block Diagram 2: This represents the part that is outside the while loop. This function writes labels the columns of an excel file.



## Appendix D: Data Files

The following chart displays experimental values for input power and plate temperature.

Power (Watts)	Voltage (V)	Current (Amps)	Temperature (°C)
58.50	50	1.17	85
84.72	60	1.41	95
115.10	70	1.64	120
150.34	80	1.88	130
190.27	90	2.11	150
238.00	100	2.38	185
317.77	116.4	2.73	240
392.69	129.4	3.03	340

The following two pictures display direct LabVIEW output data before graphical analysis.

	A	B	C	D	E	F	G	H	I	J	K	L	M	N	O	P	Q	R	S	T	U
1	Elapsed T	Nozzle Te	T0	HT1	T1	HT2	T2	HT3	T3	HT4	T4	T5	T6	V		HT6	V		Avg T	Avg K	Avg H
2	164.991	225	25.66443	32.69844	24.7186	29.01929	28.09916	29.32904	201.9539	30.01785	223.3488	221.2511	220.1218	0		29.82329	0		26.16073	216.6689	30.26
3	169.991	225	26.13664	34.32946	24.7186	28.16904	27.31512	29.64477	194.0422	28.34237	229.3442	219.1579	230.6893	0		35.4423	0.5		26.05678	218.3084	30.12
4	174.991	225	26.05797	32.88479	25.34936	29.97175	27.15816	28.32723	201.3398	28.65219	217.6674	228.8323	228.3333	0		42.04037	1		26.18849	219.0432	29.95
5	179.991	225	25.58568	32.2612	24.95523	28.25761	29.11651	29.48227	204.2557	28.83279	228.9395	220.4662	229.0315	0		48.23092	1.5		26.55247	220.6732	29.70
6	184.99	225	26.84407	32.25301	25.66443	29.8442	30.05369	29.30105	205.5594	28.86731	218.8044	222.3846	229.7296	0		54.39251	2		27.52073	219.1195	30.06
7	189.99	225	28.88193	34.77063	25.97929	30.43141	29.89762	28.12553	194.6571	29.50208	215.3924	230.9215	225.2773	0		64.28739	2.5		28.25294	216.5621	30.70
8	194.99	225	28.33413	33.78221	25.27056	29.28001	30.05369	28.6472	198.9597	30.8806	222.1321	226.4807	216.7116	0		76.951	3		27.88613	216.071	30.6
9	199.989	225	28.1775	32.48142	25.97929	29.20465	30.2877	29.50521	205.6361	30.01838	223.3488	221.3383	222.3069	0		90.27969	3.5		28.14816	218.1575	30.30
10	204.989	225	26.92261	32.36444	25.82188	29.0502	29.89762	28.81348	205.0226	30.84036	224.2407	225.8708	216.7991	0		93.28647	4		27.54737	217.9833	30.26
11	209.989	225	27.47203	33.37327	26.05797	29.2043	30.5216	28.22026	200.1883	30.30357	223.4299	230.3122	220.7337	0		115.3655	4.5		28.0172	218.666	30.27
12	214.989	225	26.29394	32.79968	25.82188	28.96736	30.13171	29.20794	202.0306	31.1417	224.8082	222.1692	215.2246	0		135.7488	5.1		27.41584	216.3081	30.52
13	219.988	225	26.29394	32.85708	25.58568	28.80412	29.35097	29.23752	201.7236	30.48024	225.6997	222.7333	218.4606	0					27.07686	217.1543	30.34
14	429.976	208	23.37544	38.6924	23.21717	30.44481	23.13802	34.61584	172.348	34.64939	212.5469	189.7337	189.4933	0.5					23.24354	191.0305	34.66
15	434.976	208	24.24498	37.34804	23.37544	30.52277	25.11292	34.81313	178.5799	35.30992	212.2216	188.9482	188.3562	0.5					24.24445	192.0265	34.45
16	439.976	208	23.29631	38.7719	23.69182	28.84662	24.56078	33.98231	171.9634	36.39524	223.511	193.3126	182.9361	0.5					23.84964	192.9308	34.45
17	444.975	208	23.69182	38.87533	23.77088	30.02975	24.32395	35.04459	171.9634	35.53794	215.7175	188.2501	186.5198	0.5					23.92889	190.6127	34.8
18	449.975	208	23.45456	38.14149	23.45456	29.4088	24.087	35.05155	174.5789	35.63956	219.4539	187.9011	185.8204	0.5					23.66537	191.9386	34.56
19	454.975	208	22.42503	37.42918	24.00799	29.66462	24.40291	33.56113	176.4254	34.82261	218.3172	195.7575	189.9306	0.5					23.61197	195.1077	33.88
20	459.975	208	22.90047	39.27885	22.97967	29.49619	23.53366	34.22615	169.6563	35.06462	218.3984	191.392	187.9189	0.5					23.13793	191.8414	34.51
21	464.974	208	23.21717	37.71741	23.13802	30.14737	23.53366	35.17045	176.0407	35.10197	214.3357	187.0287	187.744	0.5					23.29628	191.2873	34.5
22	469.974	208	24.166	38.18518	23.05885	29.49589	23.53366	34.74669	175.1174	35.19568	218.4796	188.9482	187.3068	0.5					23.58617	192.463	34.40
23	474.974	208	23.53366	38.77362	23.05885	30.25061	24.087	34.22451	172.1942	34.66485	213.604	191.4793	190.368	0.5					23.55984	191.9114	34.4

388\_Watt\_Air\_Velocity.xls [Compatibility Mode] - Excel

FILE HOME INSERT PAGE LAYOUT FORMULAS DATA REVIEW VIEW ADD-INS ACROBAT Team

Clipboard Font Alignment Number Styles Cells Editing

Q15

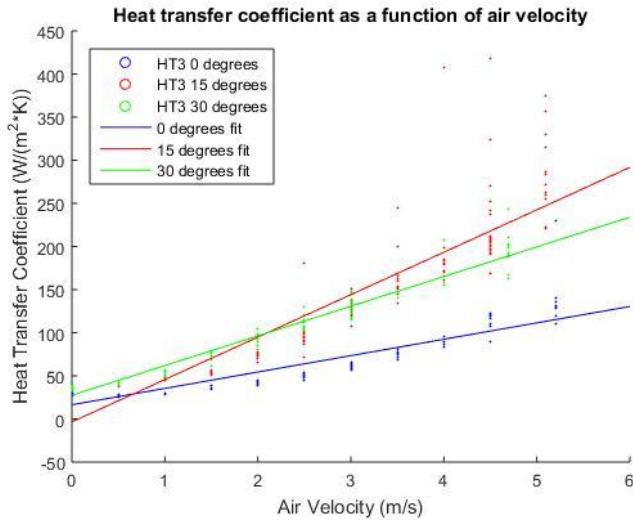
	A	B	C	D	E	F	G	H	I	J	K	L	M	N	O	P	Q	R	S	T	U
1	Elapsed Ti	Nozzle Te	T0	HT1	T1	HT2	T2	HT3	T3	HT4	T4	T5	T6	V	Power	V	HT3_D	HT4_F	HT5_H	HT6_J	
2	6088.181	340	27.47203	33.93532	29.27283	29.59852	29.03833	29.50398	304.5224	29.98289	346.9168	347.9347	342.6103	0	392.69	0	32.97975	28.34528	29.04547	30.90578	
3	6100.942	340	27.62889	32.68353	27.62889	28.23552	30.13171	29.39097	315.2904	30.59824	360.6063	347.516	337.3975	0	392.69	0.5	32.80306	29.48353	31.9128	35.32617	
4	6113.813	340	26.60838	33.08321	28.41242	28.49545	29.35097	29.09677	310.7946	31.3521	358.3526	351.5339	329.2286	0	392.69	1	39.39757	33.8692	37.63116	41.73002	
5	6126.629	340	26.84407	33.41446	27.86408	28.08498	29.27283	29.52088	308.2131	30.70583	362.6263	346.3435	335.462	0	392.69	1.5	45.63817	39.07403	44.07935	47.97808	
6	6139.734	340	27.00114	32.78833	28.80371	27.87224	29.66342	29.45288	313.7431	30.39384	366.1211	348.0184	338.9956	0	392.69	2	55.62245	46.75021	53.65061	58.78681	
7	6152.619	340	27.31512	32.41579	28.02082	28.00064	28.64723	29.54319	317.3526	32.75129	363.7915	346.2597	315.7136	0	392.69	2.5	67.34477	55.43511	64.76684	66.83371	
8	6165.558	340	27.31512	33.7901	24.48185	27.75943	29.58533	29.54137	305.5561	30.4773	363.1701	342.7404	338.0704	0	392.69	3	81.37824	65.86587	78.85765	85.58744	
9	6178.499	340	27.07965	33.61895	28.09916	28.14393	29.11651	29.58162	306.7372	32.02085	362.1602	345.9247	322.7312	0	392.69	3.5	102.9875	78.68181	96.80676	97.84494	
10	6191.462	340	26.76552	33.83101	27.7857	28.20274	29.11651	29.04044	304.6701	31.05725	361.1502	351.5339	331.8411	0	392.69	4	114.1727	89.72816	106.9059	112.8775	
11	6204.745	340	27.7073	31.01089	29.27283	27.27026	29.66342	27.49271	330.8844	31.7785	374.0364	371.2468	325.5173	0	392.69	5.3	127.4108	100.7371	130.3439	130.3163	
12	6217.73	340	27.62889	32.19727	28.02082	28.29524	29.89762	29.12996	319.6348	30.57495	360.2955	350.7808	337.3975	0	392.69						
13	6230.733	340	27.31512	31.33488	28.25582	28.98724	29.89762	29.37165	327.3575	29.27923	352.5982	348.3533	351.0056	0	392.69						
14	6243.789	340	27.7073	33.8738	28.96013	28.64423	28.64723	27.65631	305.2608	30.31896	357.1865	368.9113	338.7433	0	392.69						
15	6256.864	340	26.76552	33.30909	28.33413	29.25398	29.4291	28.21401	309.0246	31.27234	349.7192	361.5655	330.0715	0	392.69						
16	6270.141	340	27.39358	33.40962	27.7857	28.33483	30.13171	29.14592	308.8033	31.02317	359.5961	350.3624	333.1888	0	392.69						
17	6363.132	320	25.66443	31.47794	25.97929	28.30671	26.05797	32.43727	324.3432	37.10765	358.1194	315.8246	279.4233	0.5	392.69						
18	6376.362	320	23.84993	31.47274	24.7186	27.91983	25.66443	30.80767	322.578	34.74401	361.461	329.8956	296.2663	0.5	392.69						
19	6389.672	320	24.087	31.38945	23.45456	28.6253	23.92897	31.26443	323.6078	35.10532	351.8981	324.1731	291.7457	0.5	392.69						
20	6403.092	320	24.166	32.33567	23.92897	28.08079	25.66443	33.28964	314.922	35.05325	358.7412	306.353	293.879	0.5	392.69						
21	6416.392	320	24.79749	30.82707	24.166	28.41097	24.7186	34.67332	329.7825	34.88585	355.0872	295.3195	294.2202	0.5	392.69						
22	6429.75	320	24.48185	31.60185	25.11292	28.45897	25.03409	29.95597	321.9895	34.57636	355.476	338.9666	296.9479	0.5	392.69						
23	6443.299	320	23.61275	31.7289	24.00799	28.22507	24.79749	32.19021	319.9292	33.59073	357.1088	316.0779	304.6899	0.5	392.69						

388 Watt Air Velocity

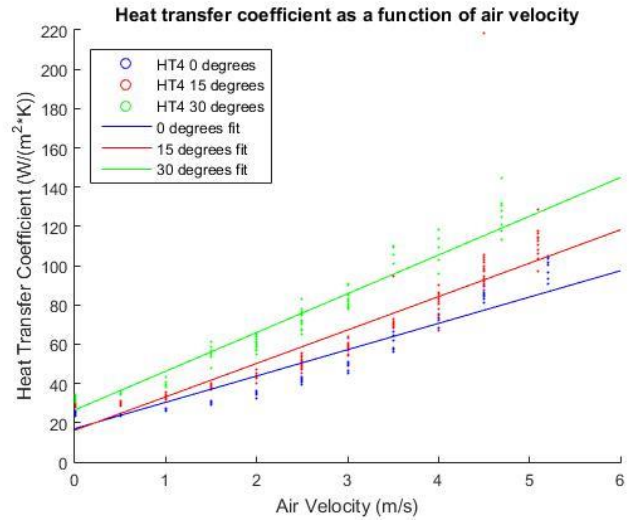
READY | 9:55 AM | 4/20/2016

## Appendix E: Additional MATLAB Generated Result's Graphs

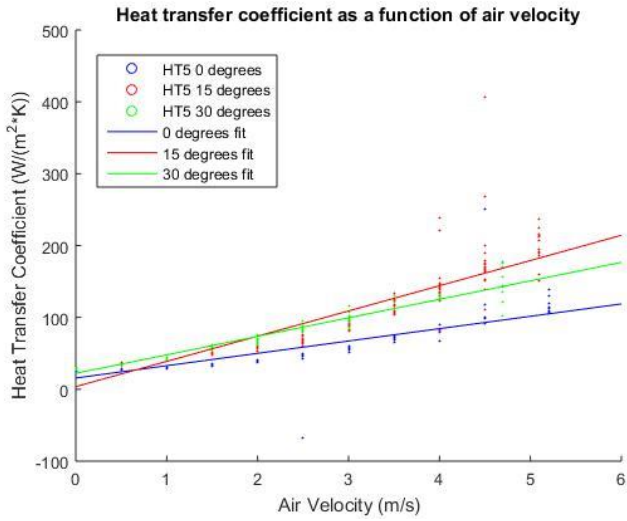
Heat Transfer Coefficient as a Function of Air Velocity for each individual thermocouple



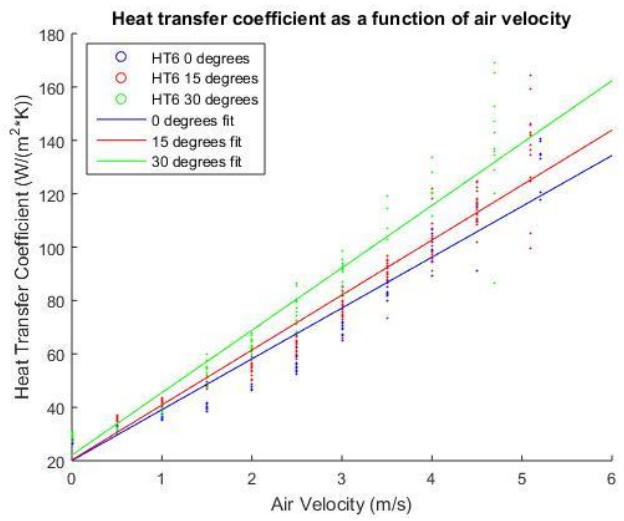
HT3



HT4

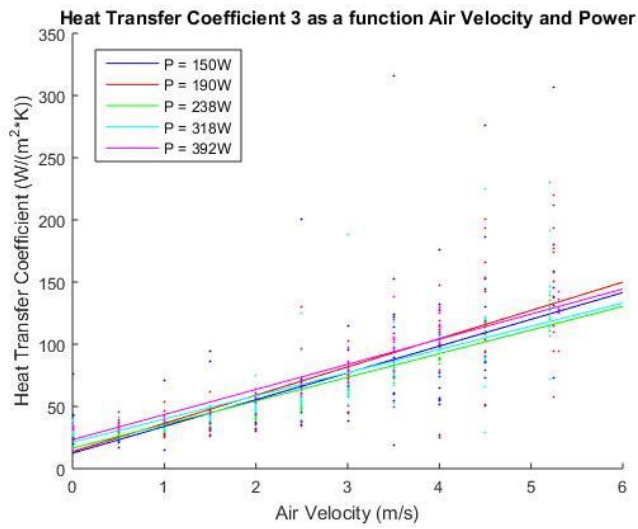


HT5

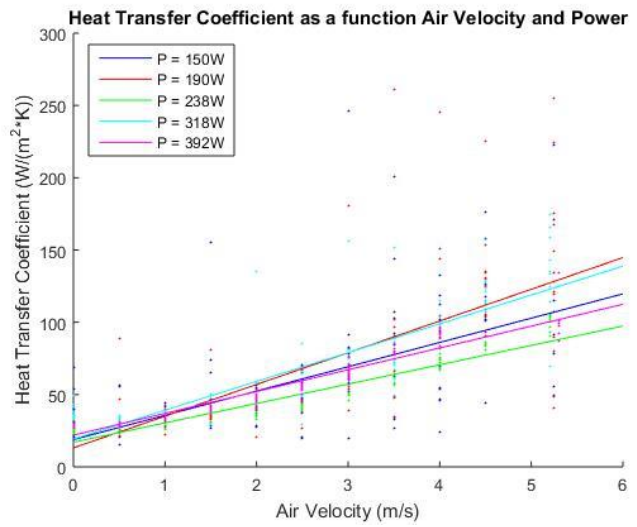


HT6

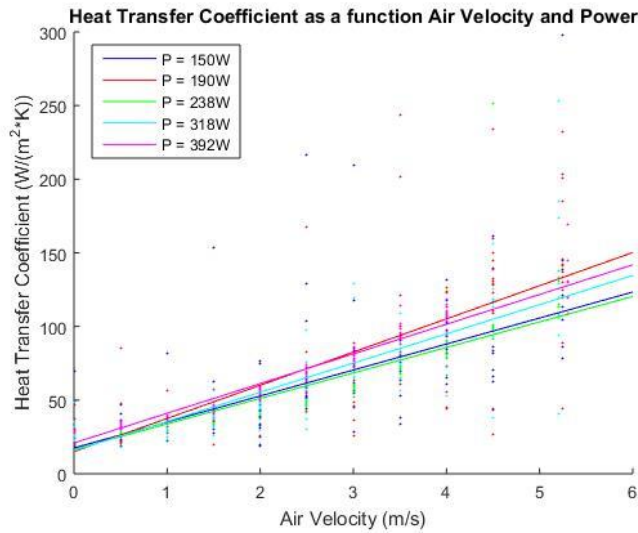
# Heat Transfer Coefficient as a function of Air Velocity and Power for each individual thermocouple



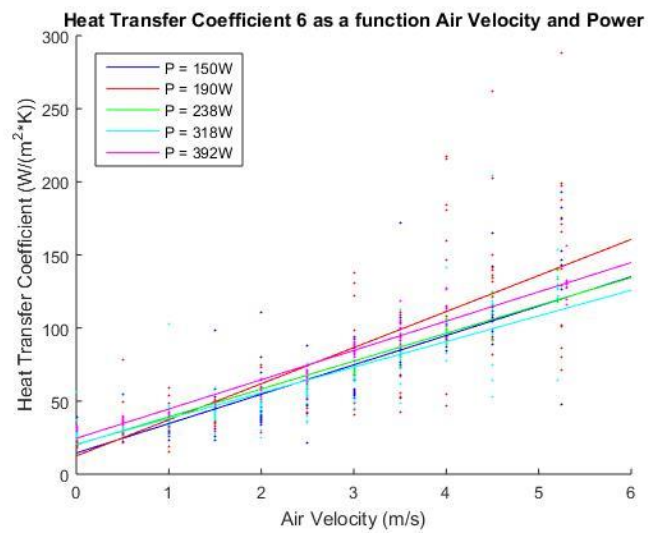
HT3



HT4

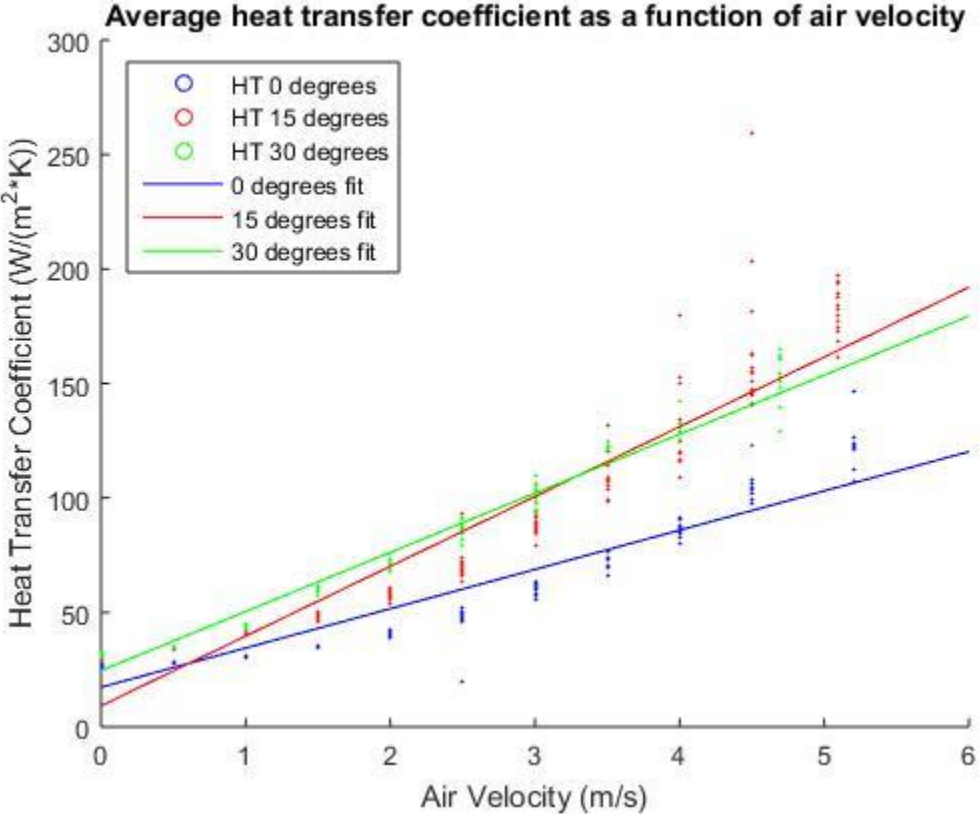


HT5



HT6

The following graph was created



Appendix F: ANSYS Generated Fluent Report



**Title**

ME MQP

**Author**

FL, RW, JMV, KL

**Date**

2016/04/18 13:44:14

---

## Contents

[1. File Report](#)

[Table 1](#) File Information for MQP 2D

[2. Mesh Report](#)

[Table 2](#) Mesh Information for MQP 2D

[3. Physics Report](#)

[Table 3](#) Domain Physics for MQP 2D

[Table 4](#) Boundary Physics for MQP 2D

[4. User Data](#)

[Chart 1](#)

[Chart 2](#)

[Figure 1](#) Velocity Profile

[Figure 2](#) Turbulance Check

[Figure 3](#) Pressure Gradient

---

# 1. File Report

**Table 1.** File Information for MQP 2D

<b>Case</b>	MQP 2D
<b>File Path</b>	C:\Users\frlee\Desktop\MQP\FLUENT\2d_files\dp0\FFF\Fluent\FFF.1-13-01500.dat.gz
<b>File Date</b>	25 February 2016
<b>File Time</b>	03:18:11 PM
<b>File Type</b>	FLUENT
<b>File Version</b>	16.2.0

## 2. Mesh Report

**Table 2.** Mesh Information for MQP 2D

Domain	Nodes	Elements
surface_body	9362	4500

### 3. Physics Report

**Table 3.** Domain Physics for MQP 2D

Domain - surface_body	
Type	cell

**Table 4.** Boundary Physics for MQP 2D

Domain	Boundaries
surface_body	<b>Boundary - centerline</b>
	Type AXIS
	<b>Boundary - inlet</b>
	Type VELOCITY-INLET
	<b>Boundary - outlet</b>
	Type PRESSURE-OUTLET
	<b>Boundary - symmetry 1</b>
	Type SYMMETRY
	<b>Boundary - symmetry 2</b>
	Type SYMMETRY
	<b>Boundary - topwall</b>
	Type WALL

### 4. User Data

Chart 1.

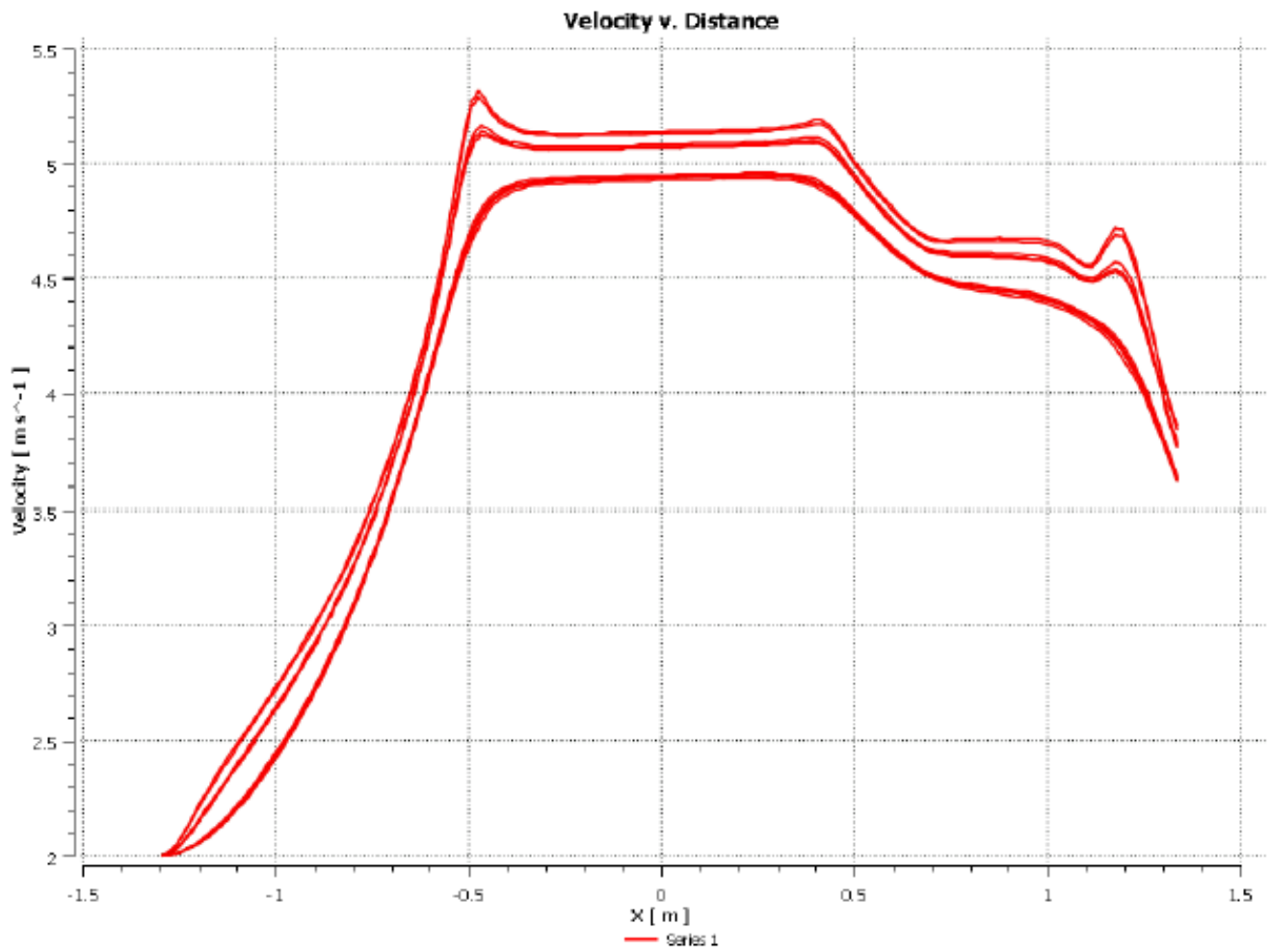


Chart 2.

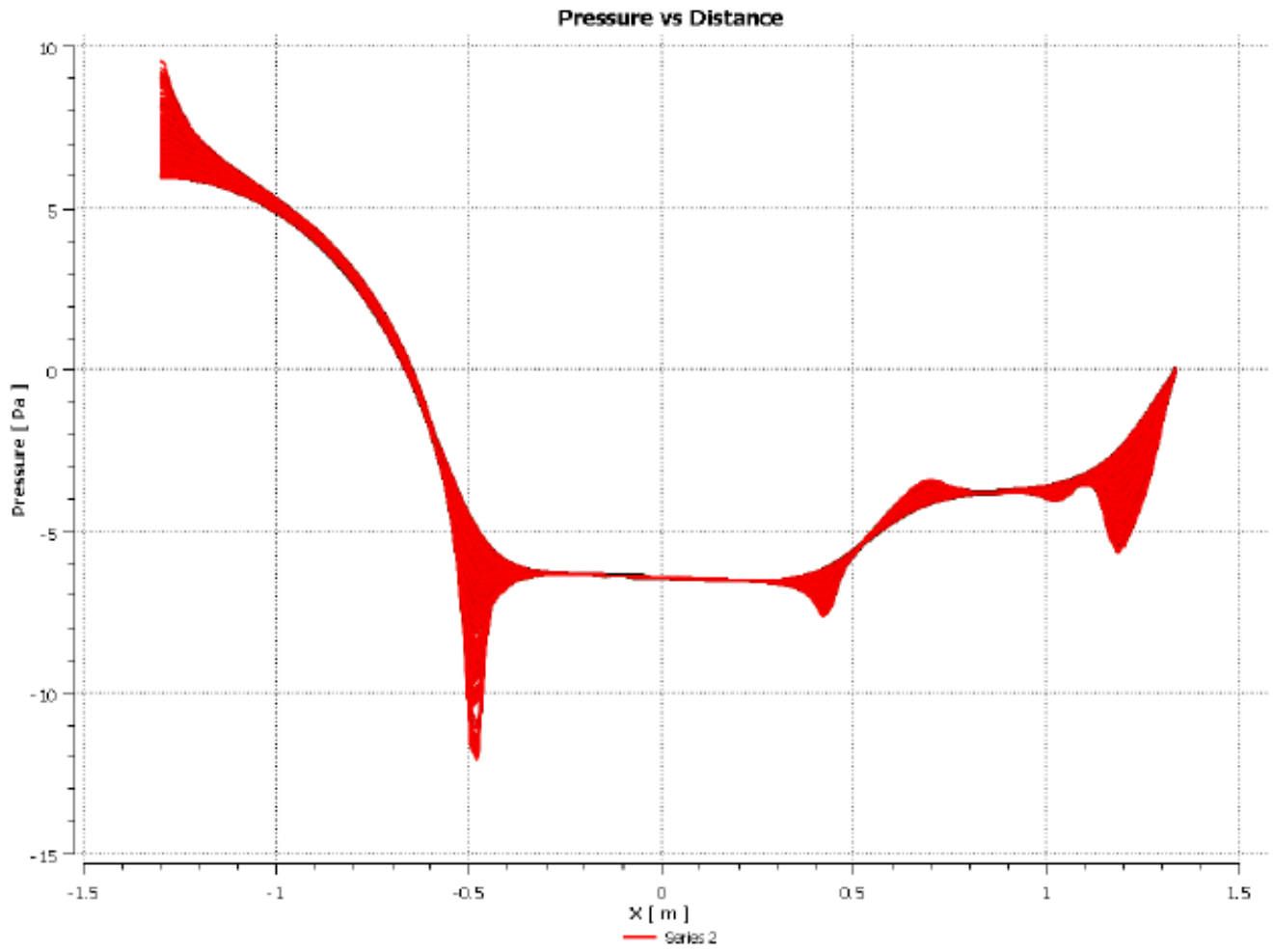


Figure 1. Velocity Profile

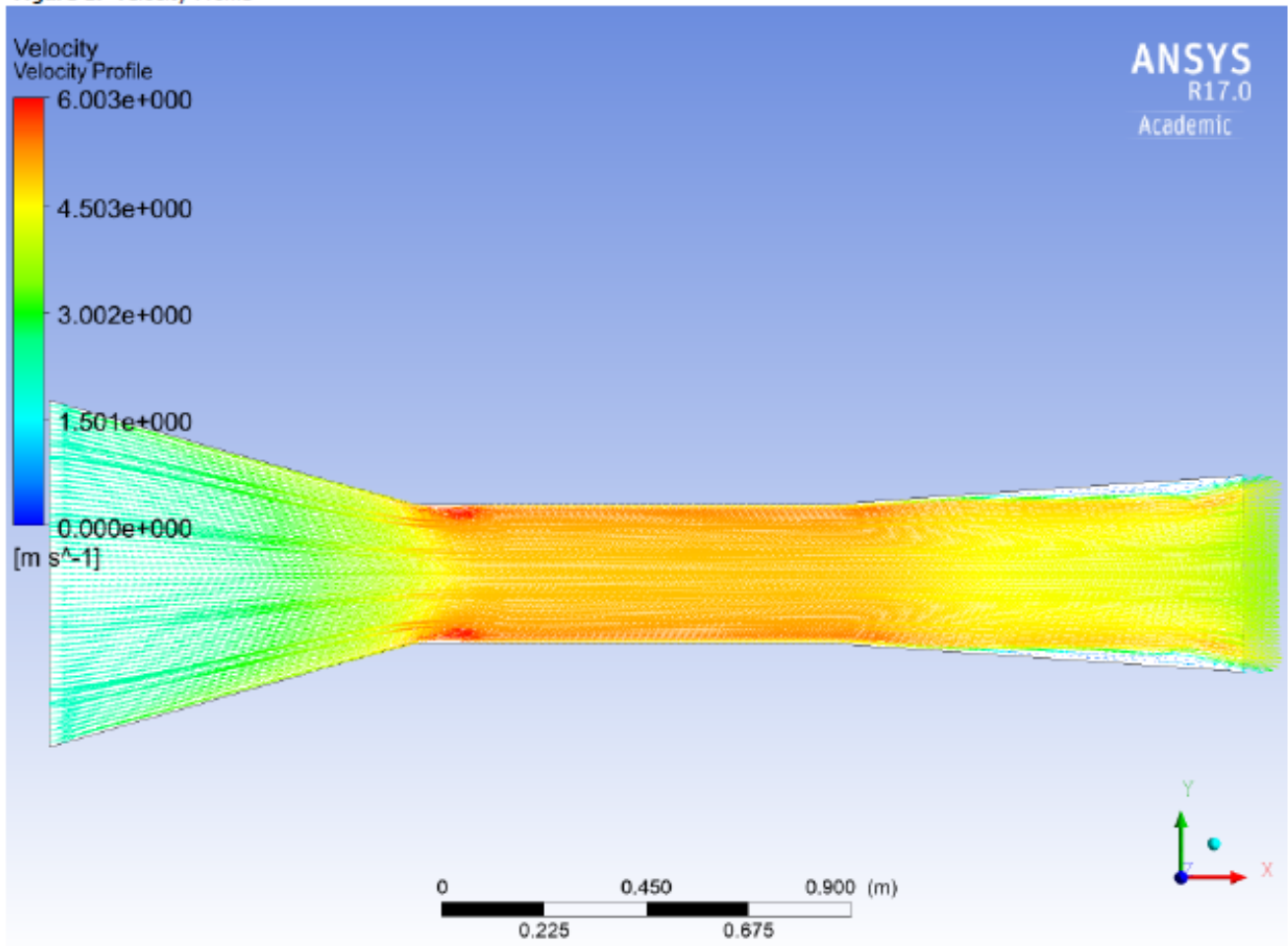




Figure 2. Turbulence Check

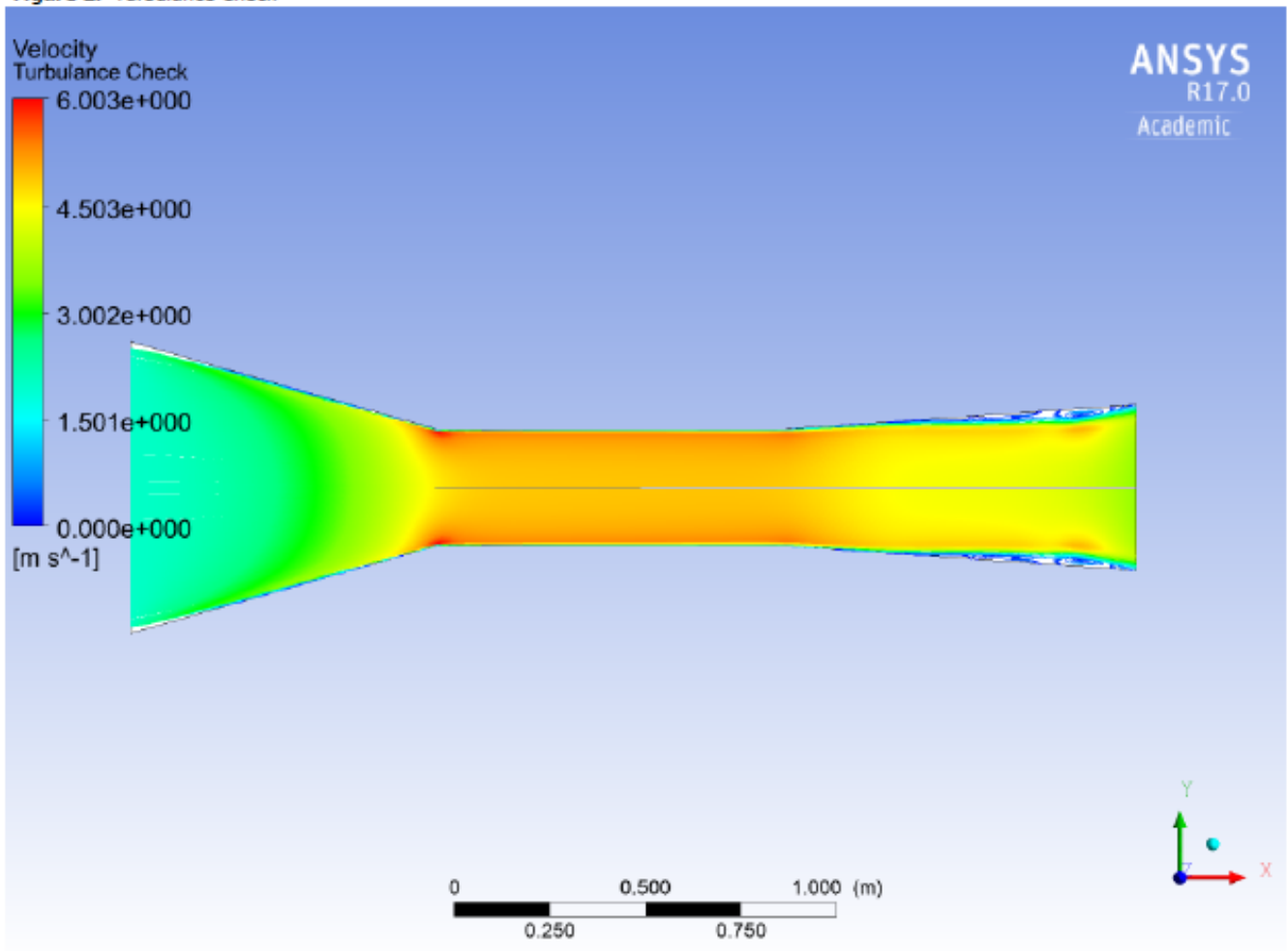
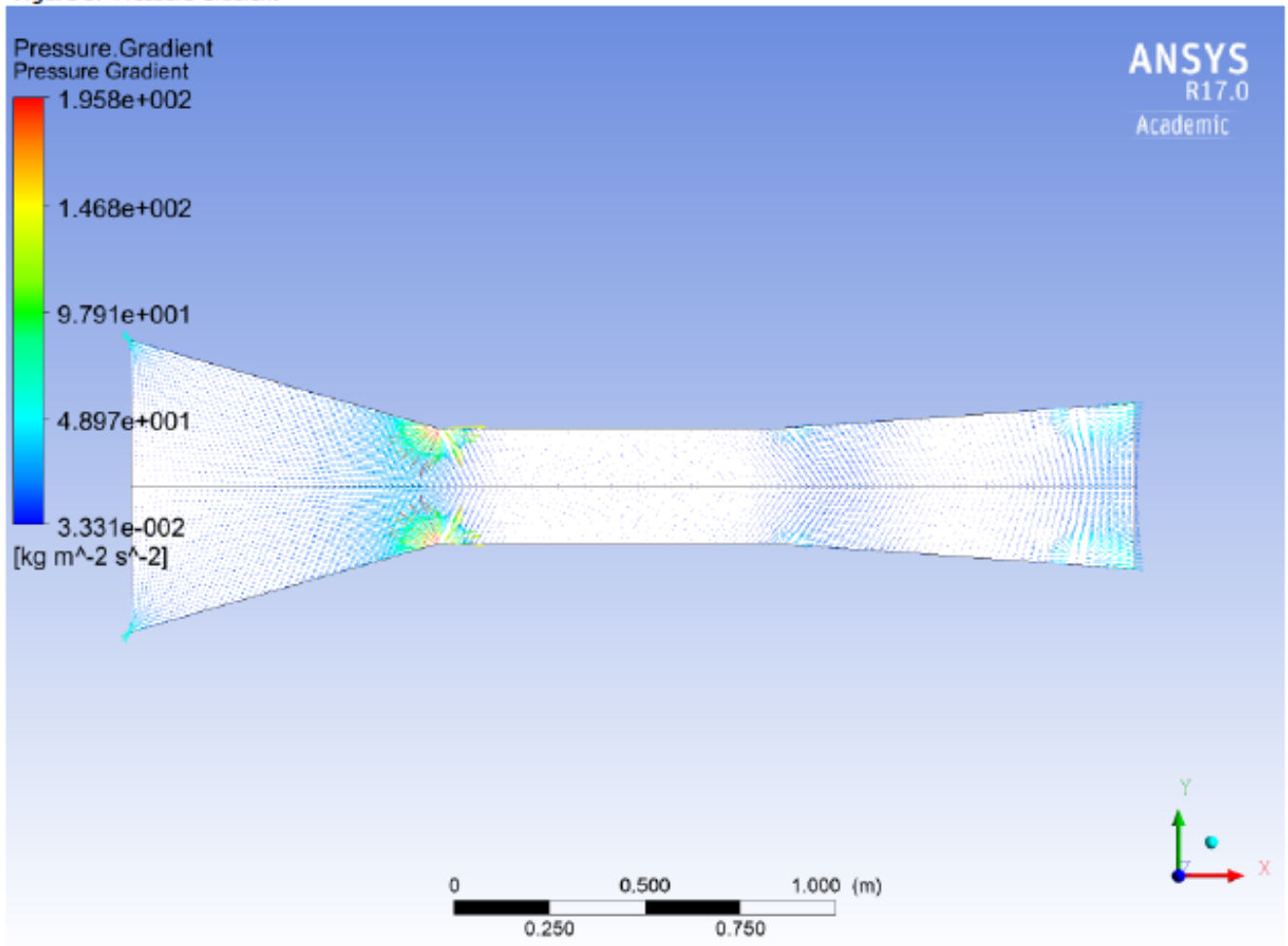
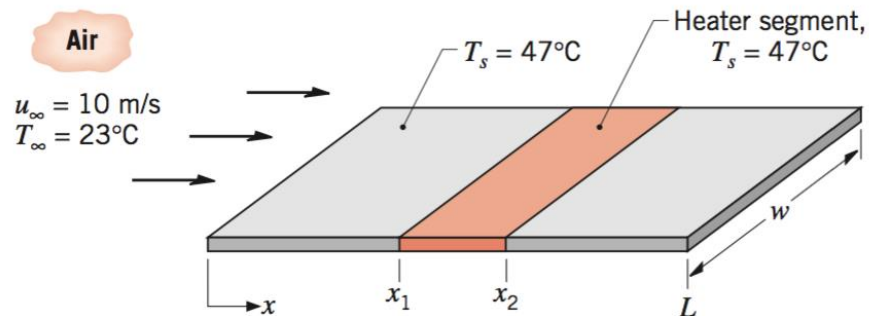


Figure 3. Pressure Gradient



## Appendix G: Textbook Sample Problem

**9.48** A highly polished aluminum plate of length 0.5 m and width 0.2 m is subjected to an airstream at a temperature of 23°C and a velocity of 10 m/s. Because of upstream conditions, the flow is turbulent over the entire length of the plate. A series of segmented, independently controlled heaters is attached to the lower side of the plate to maintain approximately isothermal conditions over the entire plate. The electrical heater covering the section between the positions  $x_1 = 0.2$  m and  $x_2 = 0.3$  m is shown in the schematic.



- Estimate the electrical power that must be supplied to the designated heater segment to maintain the plate surface temperature at  $T_s = 47^\circ\text{C}$ .
- If the blower that maintains the airstream velocity over the plate malfunctions, but the power to the heaters remains constant, estimate the surface temperature of the designated segment. Assume that the ambient air is extensive, quiescent, and at 23°C.